

Star cluster ecology V: Dissection of an open star cluster—spectroscopy

Simon F. Portegies Zwart,^{1*} Piet Hut,² Stephen L. W. McMillan³ and Junichiro Makino,⁴

¹ *Astronomical Institute 'Anton Pannekoek', University of Amsterdam, Kruislaan 403, 1098SJ Amsterdam, the Netherlands,*

Section Computational Science, University of Amsterdam, Kruislaan 403, 1098SJ Amsterdam, the Netherlands

² *Institute for Advanced Study, Princeton, NJ 08540, USA*

³ *Department of Physics, Drexel University, Philadelphia, PA 19104, USA*

⁴ *Department of Information Science and Graphics, College of Arts and Science, University of Tokyo, 3-8-1 Komaba, Meguro-ku, Tokyo 153, Japan*

Accepted 2145 December 32. Received 1687 December -1; in original form 1900 October 11

ABSTRACT

We have modeled in detail the evolution of rich open star clusters such as the Pleiades, Praesepe and Hyades, using simulations that include stellar dynamics as well as the effects of stellar evolution. The dynamics is modeled via direct N -body integration, while the evolution of single stars and binaries is followed through the use of fitting formulae and recipes. The feedback of stellar and binary evolution on the dynamical evolution of the stellar system is taken into account self-consistently.

Our model clusters dissolve in the tidal field of the Galaxy in a time span on the order of a billion years. The rate of mass loss is rather constant, $1 \sim 2 M_{\odot}$ per million years. The binary fraction at first is nearly constant in time, then increases slowly near the end of a cluster's lifetime. For clusters which are more than about 10^8 years old the fractions of stars in the form of binaries, giants and collision products in the inner few core radii are considerably higher than in the outer regions, beyond the cluster's half mass radius. When stars with masses $\gtrsim 2 M_{\odot}$ escape from the cluster, they tend to do so with velocities higher than average.

The stellar merger rate in our models is roughly one per 30 million years. Most mergers are the result of unstable mass transfer in close binaries ($\sim 70\%$), but a significant minority are caused by direct encounters between single and binary stars. While most collisions occur within the cluster core, even beyond the half mass radius collisions occasionally take place. We notice a significant birthrate of X-ray binaries, most containing a white dwarf as the donor. We also find some X-ray binaries with a neutron-star donor, but they are relatively rare. The persistent triple and higher order systems formed in our models by dynamical encounters between binaries and single stars are not representative for the multiple systems observed in the Galactic disk or in open clusters. We conclude that the majority of multiples in the disk probably formed when the stars were born, rather than through later dynamical interactions.

Key words: Methods: N-body simulations – Binaries: general – Binaries: close – Open cluster and associations: general – Open cluster and associations: NGC2516, NGC2287, Praesepe, Hyades, NGC 2660, NGC 3680

1 INTRODUCTION

Open clusters are useful laboratories for studying the interplay between single star evolution, binary star evolution and stellar dynamics. Unlike their bigger (and older) siblings, the globular clusters, they contain a manageable number of stars, and the evolution of the majority of the stars is not expected to be strongly affected by the dynamics. Still, a

significant number of collisions and subsequent stellar mergers can take place, as well as dynamically induced exchange reactions between single stars and binaries. For all these reasons, the usual zoo of objects created in binary stellar evolution is significantly enlarged by the presence of even more exotic specimens that could not have formed *in vitro* through isolated evolution, but only *in vivo* through the dynamical interplay of initially unrelated (single or multiple) stars.

* E-mail: spz@science.uva.nl; KNAW fellow

The simulations reported here have been run on a

Table 1. Observed and derived parameters for several open star clusters with which our simulations may be compared. References to the literature (second column) are: (a) Pinfield et al. (1998); Raboud & Mermilliod, (1998); Bouvier et al (1998); (b) Abt & Levy (1972); Dachs, J & Kabus (1989); Hawley et al. (1999). (c) Harris et al. (1993); Ianna et al (1987); Cox (1954). (d) Andrievsky (1998); Jones & Stauffer (1991); Mermilliod & Mayor (1999); Mermilliod et al. (1990); Hodgkin et al. (1999). (e) Perryman et al. (1998 and references therein) Reid & Hawley (1999); (f) Frandsen et al. (1989); Hartwick & Hesser (1971); Sandrelli et al. (1999). (g) Hawley et al. 1999 ; Nordström et al. (1997); Nordström et al. (1996), Subsequent columns give (3) the distance to the cluster (in pc), (4) the cluster age (in Myr), (5) the half mass relaxation time, (6) the crossing time, (7) the total mass (in M_{\odot}), (8) estimate for the half mass radius (in pc), and (9) the core radius. In cases where the relaxation time is not given in the literature, we calculate it (see Paper IV); these entries are indicated by *. The final two columns contain information about cluster stellar content. The column labeled $f_{s:b:t}$ indicates the number of single stars, binaries and triples (separated by colons). For clusters where the numbers are given directly by observations, the table gives the observed numbers of each system. If the binary fraction is derived by other methods, we give the relative fractions normalized to the number of single stars. The last column ($N_{bss:Be:gs}$) gives the number of observe blue stragglers, Be stars and giants, separated by a column.

name	ref.	d [pc]	t — [Myr] —	t_{rlx} (5)	t_{hm} (6)	M [M_{\odot}] (7)	r_{tide} (8)	r_{hm} — [pc] — (9)	r_{core} (10)	$f_{s:b:t}$ (11)	$N_{bss:Be:gs}$ (12)
Pleiades	a	135	115	150	8	~ 1500	16	2–4	1.4	137:60:2	3:3:?
NGC2516	b	373	110	220		1000		2.9		16:6:?	6:3:4
NGC2287	c	675	160–200	—			6.3			1:0.6:?	3:1:8
Praesepe	d	174	400–900	220		1160		12	2.8	1:0.3:0.03	?:5:?
Hyades	e	46	625	320	15	1027	10.3	3.7 ¹	2.6	1:0.4:0	1:0:4
NGC 2660	f	2884	900–1200	260		400	?	4	~ 1	0:0.3:?	18:4:39
NGC 3680	g	735	1450	28		100	4.3	1.2	~ 1	44:25:0	4:4:17

Table 2. Initial conditions and parameters for the selected models. The first column gives the model name, followed by the cluster mass (in M_{\odot}), the King (1966) parameter W_0 , the distance to the Galactic center (in kpc), the initial relaxation time and half mass crossing time (both in Myr). The remaining columns give the location of the cluster’s Jacobi surface along the $X-$ (towards the Galactic center), $Y-$ and $Z-$ (towards the Galactic pole) axes, and the initial virial radius, half mass radius and core radius (all in parsec).

name	M [M_{\odot}]	W_0	R_{Gal} [kpc]	t_{rlx} [Myr]	t_{hm}	r_{Jacob} [pc]	r_{vir}	r_{hm} [pc]	r_{core}		
W4	1708	4	6.8	135	4.07	14.5	9.7	7.2	2.5	2.14	0.83
W6	1603	6	10.4	140	4.15	21.6	14.4	10.8	2.5	2.00	0.59

GRAPE-4 (Makino et al. 1997) system, a special-purpose computer designed to speed up stellar-dynamical calculations. While the models in this paper contain only $\sim 3,000$ stars, appropriate for open clusters, we have started to use the next-generation special-purpose computer, the GRAPE-6, to extend our simulations to include one or two orders of magnitude more stars. This will enable us to model globular clusters on a star-by-star basis, including those with very dense cores where most stars are influenced by various ‘traffic accidents’ in the form of encounters and mergers. The simulations reported here thus play a double role: astrophysically, they provide insight in the evolution of open clusters, and computationally, they help pave the way for the modeling of the more complex globular clusters.

In this paper we describe a series of self-consistent simulations of the evolution of open star clusters. All important effects are included to some degree of realism: stellar evolution, binary evolution, the internal dynamical evolution and the effects of the tidal field of the Galaxy. This is the fifth paper in a series in which we have gradually increased the ‘ecological’ complexity of stellar interactions to a realistic level. In this paper we analyze the results of the same eight calculations performed for our previous Paper IV (Portegies Zwart et al. 1999). There we concentrated on global

cluster properties and compared them with observed open clusters, such as the Pleiades, Praesepe and Hyades. Specifically, we took a photometric standpoint and studied changes in the Hertzsprung-Russell diagram and cluster morphology as functions of time and initial conditions. Here we concentrate on the binary population and on higher-order multiple systems, and we study the dynamical and observational effects of these binaries and multiples on the evolution of the stellar system as a whole.

Detailed descriptions of the numerical methods used and global assumptions made in our calculations are given in Paper IV. Since we analyze the same data from a different perspective we do not repeat this information here. Instead, we quickly review the initial conditions of our models, and restate the methods used; for more details, see Paper IV.

2 METHODS

In this section we briefly discuss the initial conditions of our models and the numerical techniques used in our model calculations. For details, refer to Appendix B and C of Paper IV (Portegies Zwart et al. 1999).

Table 3. Initial conditions for the stellar and binary population. The first column gives the parameter, the second column gives the functional dependence, followed by the lower and upper limits adopted. (RLOF indicates that the initial binary may be semi-detached.)

parameter	function	lower	upper
		limits	
mass function	Scalo	$0.1 M_{\odot}$	$100 M_{\odot}$
secondary mass	$P(m) = \text{constant}$	$0.1 M_{\odot}$	$M_{\text{prim}}/M_{\odot}$
orbital separation	$P(a) = 1/a$	RLOF	5000 AU
eccentricity	$P(e) = 2e$	0	1

2.1 Initial conditions

We are interested in moderately rich (~ 1000 stars) open clusters of intermediate age ($\lesssim 1$ Gyr). Starting from the currently observed mass and dynamical properties of such clusters we have reconstructed two plausible sets of initial conditions, which are presented in Table 2. Each calculation is performed four times with different random seeds in order to improve statistics. The notation in this paper is identical to that used in Paper IV (see its Appendix A for an overview).

For our simulations we assume a Scalo (1986) initial mass function, with minimum and maximum masses of $0.1 M_{\odot}$ and $100 M_{\odot}$, respectively, and mean mass $\langle m \rangle \simeq 0.6 M_{\odot}$ at birth. Consistent with the above mass estimates, our simulations are performed with 1024 single stars and 1024 binaries, for a total of 3096 (3k) stars.

Stars and binaries within our model are initialized as follows. A total of 2k single stars are selected from the initial mass function and placed in an equilibrium configuration in the selected density distribution (see below). We then randomly select 1k stars and add a second companion star to them. The masses of the companions are selected randomly from the IMF between $0.1 M_{\odot}$ and the primary mass (see Tab. 3). For the adopted binary fraction, the restricted secondary mass range translates into an overall mean mass of $0.53 M_{\odot}$. Then the other binary parameters are determined. Binary eccentricities are selected from a thermal distribution between 0 and 1. Orbital separations a are selected with uniform probability in $\log a$ between Roche-lobe contact and an upper limit of 5,000 A.U. ($= 10^6 R_{\odot}$, or 0.02 pc). When a binary appears to be in contact at pericenter, that particular orbit choice is rejected and new orbital parameters are selected. Table 3 gives an overview of the various distribution functions from which stars and binaries are initialized. (Figure 4 shows the initial distributions of orbital period and eccentricity.)

We select initial density profiles from the density distributions described by Heggie & Ramamani (1995) with $W_0 = 4$ and $W_0 = 6$, and refer to these models as W4 and W6, respectively, throughout this paper. We have performed four independent simulations for each set of initial conditions, labeled *I* to *IV*.

All our cluster models start with the same virial radius of $R_0 = 2.5$ pc. This implies a conveniently constant scaling between the cluster dynamical time scale $\sim (GM_0/R_0^3)^{-1/2}$ ($= 1.5$ Myr for $M_0 = 1600 M_{\odot}$) and the time scale for stellar evolution. Each cluster is assumed to precisely fill its Jacobi surface at birth. Given the observed Oort constants in the

solar neighborhood, we find that a model with $W_0 = 6$ has to be placed slightly farther (10.4 kpc) from the Galactic center than the Sun, while a model with $W_0 = 4$ has to reside somewhat closer (6.8 kpc), in order to obey the above relationships.

For a total cluster mass of $1600 M_{\odot}$, the Lagrange points of our two standard clusters lie at distances 14.5 pc ($W_0 = 4$) and 21.6 pc ($W_0 = 6$), from the cluster center. Stars are removed from a simulation when their distance to the cluster’s density center exceeds twice the distance to the first Lagrangian point. Table 2 reviews the selected parameters and initial conditions.

2.2 The *N*-body integrator

The *N*-body integration in our simulations is carried out using the *kira* integrator, operating within the Starlab software environment (McMillan & Hut 1996; Portegies Zwart et al. 1999). *Kira* uses a fourth-order Hermite scheme (Makino & Aarseth 1992), incorporates block time steps (McMillan 1986a; 1986b; Makino 1991), includes special treatments of close two-body and multiple encounters of arbitrary complexity, and a robust treatment of stellar and binary evolution and stellar collisions (see below). As mentioned above, the special-purpose GRAPE-4 (Makino et al. 1997) system is used to accelerate the computation of gravitational forces between stars.

2.3 Stellar evolution

The evolution of the stars is adapted from the prescription by Portegies Zwart & Verbunt (1996, §2.1). However, some changes are made to the mass loss in the main-sequence stage for massive stars and for mass-transfer remnants. We follow the details of model B from Portegies Zwart & Yungelson (1998). For our treatment of stellar mass loss, see Portegies Zwart et al. (1998).

Neutron stars receive a high-velocity kick at the moment of their formation. The reasons for the occurrence of these high kick velocities have been discussed in detail by Portegies Zwart & van den Heuvel (1999) and the implications for binary evolution are discussed by Portegies Zwart (2000). The distribution from which the kick velocity should be taken is less certain. We adopt the velocity distribution proposed by Harmann (1997) which has a dispersion velocity of 450 km s^{-1} . Each neutron star formed received a kick chosen from this distribution and oriented in a random direction.

3 RESULTS

3.1 Overall evolution of the models

In this section we review the global properties of models W4 and W6, summarizing the more extensive discussion presented in Paper IV. Where we discuss individual models, we focus on the same two models discussed in Paper IV (model W4-IV and W6-III). In other cases the data for several models, or even all models, are combined in order to improve statistics; those cases are indicated specifically below.

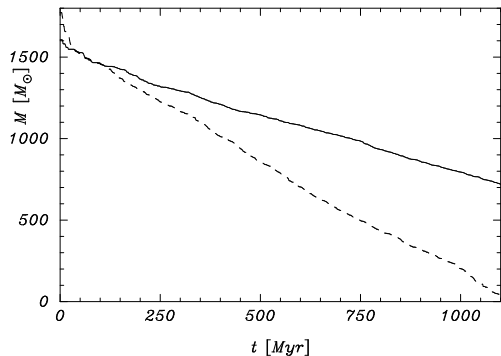


Figure 1. Total mass as a function of time for model W4 (dashes) and W6 (solid).

Figures 1 and 2 present the overall evolution for our two sets of cluster initial conditions. Figure 1 shows the time evolution of the cluster mass. Models W4 and W6 lose mass at roughly constant rates of about $1.4 M_{\odot}$ (0.09%) and $0.82 M_{\odot}$ (0.05%) per million years, respectively. These mass loss rates result in the disruption of the cluster at about 1 Gyr for model W4 and around 2 Gyr for the more concentrated model W6. The higher mass loss rate of model W4 is mainly attributable to its closer proximity to the Galactic center and not per se to its lower concentration. These rates are consistent with a mass loss rate of $1.2 M_{\odot}$ per million years for the slightly more massive star cluster studied by Hurley et al. (2001; 2002). The mass-loss rates per half mass relaxation time derived by Portegies Zwart et al. (2001) for dense star clusters near the Galactic center are about a factor of four higher than the corresponding rates for the clusters studied here.

Figure 2 shows the evolution of the Lagrangian radii containing 5%, 25%, 50% and 75% of the cluster mass, for models W4 and W6. Both clusters expand by about a factor of three during the first half-mass relaxation time (~ 140 Myr). It is not clear whether the clusters experience any significant core collapse during this early phase. In Paper IV we concluded that the clusters do not experience core collapse due to the effects of binary activity, which tends to counteract core contraction (see McMillan et al. 1990, 1991). At later times ($t \gtrsim 650$ Myr for model W4 and somewhat later for model W6), the Lagrangian radii decrease again as the cluster starts to dissolve in the tidal field of the Galaxy.

3.2 Global binary properties

Both models start with 50% binaries, so two-thirds of the stars are initially members of binary systems. The adopted upper limit ($10^6 R_{\odot}$) on the initial semi-major axis means that most initial binaries are relatively wide. The fraction of hard ($|E| \gtrsim 1kT$) binaries was 0.46 ± 0.01 for all models, irrespective of the initial density profile. (The thermodynamic unit kT is defined in Paper IV).

Figure 3 shows the evolution of the binary fraction. Shortly after the start of the runs, the binary fractions drop to about 42% and 48% for models W4 and W6, respectively, and remain roughly constant thereafter. This initial decrease

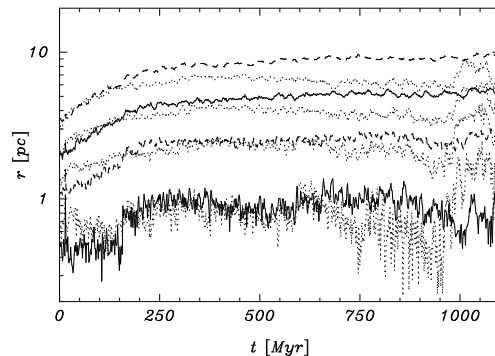


Figure 2. Evolution of the 5%, 25%, 50% and 75% Lagrangian radii for model W6 (solid lines for the 5% and 50%, dashed lines for the 25% and 75% Lagrangian radii). Lagrangian radii for model W4 are presented as dotted lines.

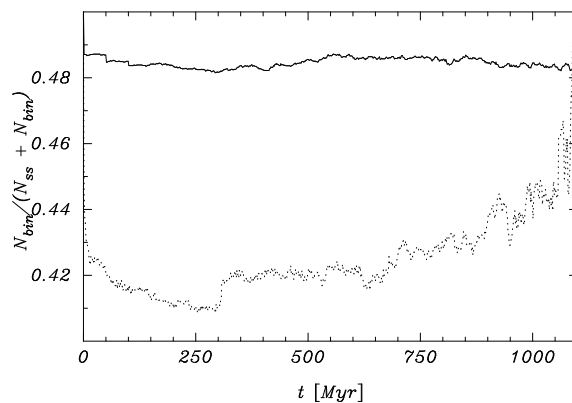


Figure 3. Binary fractions as a function of time for models W4 (dotted line) and W6 (solid line).

in binary frequency is consistent with the disruption of all soft ($|E| \lesssim 1kT$) binaries. Supernova explosions dissociated 1.8% of the binaries in the W4 models, and about half that number in the W6 models. This difference is mainly the result of random fluctuations. Fluctuations in the binary fraction after ~ 100 Myr are mainly the result of escapers and mergers. The number of mergers resulting from unstable mass transfer or direct collisions is $12.1 \pm 0.5\%$ for models W4 and W6. The escape rate of binaries closely follows the escape rate of single stars; both are relatively constant with time. Model W6 loses one binary per 2Myr; the escape rate for model W4 is about twice as high.

3.3 Evolution of binary parameters

The ecological interplay between stellar (and binary) evolution, stellar (and binary) dynamics, and the external tidal influence of the Galaxy transforms the initial distributions of stars and binaries in complex ways. We assume that initially all binaries are distributed throughout the cluster in the same way as single stars. However, since binaries are on average more massive than single stars, they subsequently tend to sink to the cluster center, where superelastic encoun-

ters quickly modify the spatial distributions of both stars and binaries.

These encounters come in many forms, from the more common single-star–binary and binary–binary types to the rare forms that involve triples and occasionally even higher-order multiple systems. The combined effects of such encounters significantly modifies the binary distribution functions, in terms of radius and binding energy as well as stellar type. In addition, stellar evolution and isolated binary evolution also cause binary parameters to evolve in time, independent of the occurrence of dynamical close encounters. In this subsection, we will present some of the net results of these complex processes.

3.3.1 Distributions of orbital period and eccentricity

Figure 4a shows the initial distribution of orbital period (in years) and eccentricity of a subset of the primordial binaries of model W6 (the initial conditions for model W4 are identical). Figures 4b and c show the same distributions for models W4 (panel b) and W6 (panel c) at 600 Myr. In the middle panel, for model W4, only 871 binaries remained. In order to facilitate visual comparison, the upper and lower panels also show only 871 binaries out of the larger numbers that could have been plotted.

A striking feature of the three panels in Fig 4, is the lack of wide ($p_{\text{orb}} \gtrsim 10^4$ yr) binaries at later times. These binaries are completely absent in model W4, while in model W6 a small population of wide binaries remains. This deficiency in wide binaries in evolved clusters is caused by ionization of the soft binaries by dynamical encounters (see also Figure 3). For model W4 this process is more efficient than for the more concentrated models because 1) the W4 models experience a high density phase during their early evolution, and 2) the W6 models have extended outer regions with relatively low stellar densities because of the weaker tidal field. All surviving binaries with $p_{\text{orb}} \gtrsim 10^5$ year are located well beyond the cluster’s half mass radius, and most contain at least one white dwarf. In many cases, the orbital periods of these non-interacting binaries has increased substantially due to the large amount of mass lost from one (or both) of the component stars.

Binaries located above and to the left of the left-most dotted curves experience strong tidal effects during their early evolution. As a result, they quickly circularize, as can be seen by their precipitation to the zero-eccentricity line at the bottom in the last two panels. The majority of these systems contain at least one white dwarf or helium star. Occasionally a binary may enter the ‘forbidden’ left-most area at a later time as a result of a strong dynamical encounter. Such a binary will either be quickly circularized or its components will collide and merge to form a single star (see §3.5).

Figure 5 shows how the percentage of tidally circularized binaries evolves over time. Not surprisingly, the very hard binaries, which have high binding energy and therefore tight orbits, have on average undergone much stronger tidal interactions and therefore have had a much larger chance to circularize. The four percentages presented in the figure—hard binaries and all binaries for each of the two classes of model—at first change little during the evolution of the

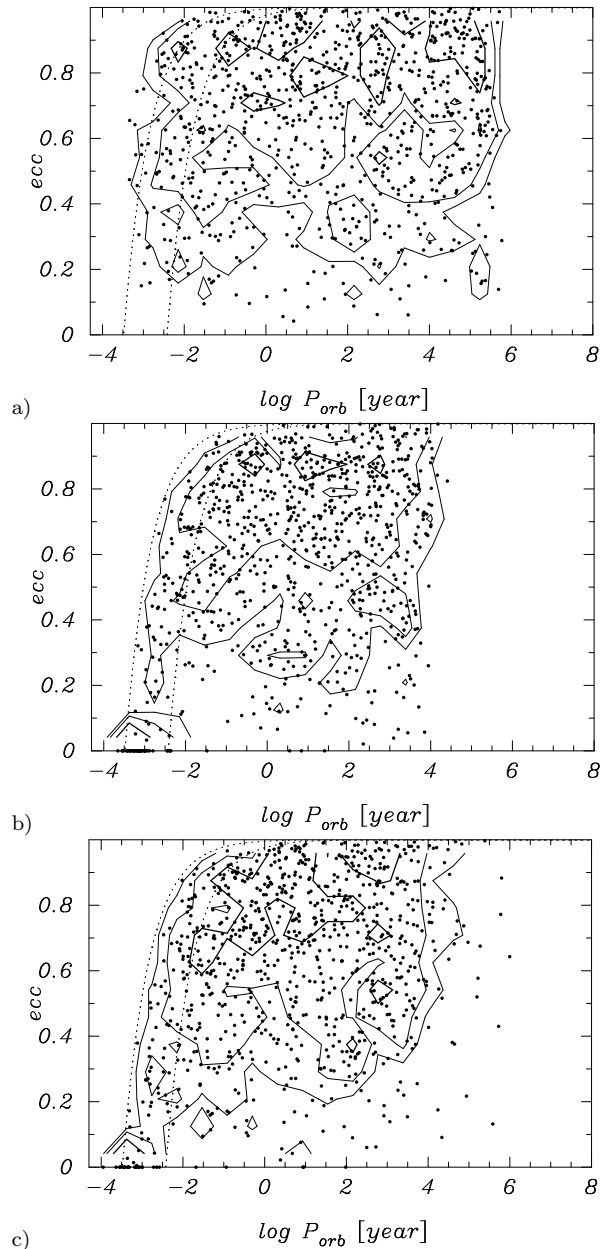


Figure 4. Scatter plots for the orbital period versus the eccentricity for 871 binaries for various models and moments in time: a) initial distribution, b) the distribution for model W4 at an age of 600 Myr, c) model W6 at $t = 600$ Myr. Each panel is constructed using 871 binaries. Contours give the 0.5, 0.25 and 0.125 iso-density curves of the distribution in the two coordinates plotted here. The left dotted curve indicates at which orbital period and eccentricity a binary with a $0.1 M_{\odot}$ zero-age primary circularizes during the time span of our simulations. The right dotted curve is for a $2.26 M_{\odot}$ primary at zero age.

cluster, but they increase at later times in the case of model W4.

Note that in Fig 4 there are some circularized binaries with long orbital periods, far to the left of the right-most dotted line, in the middle and lower panel. These are absent in the upper panel, which shows the initial conditions. The tidal circularization of these systems occurred when one of the stars ascended the giant branch before the onset of mass

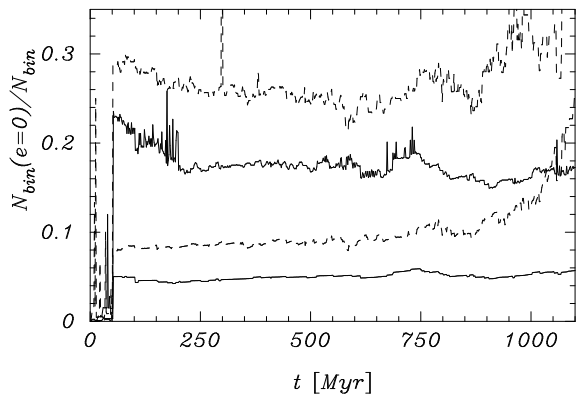


Figure 5. The relative number of binaries that are tidally circularized, as a function of time, for the models W4 (dashed lines) and W6 (solid lines). In each case, the lower lines present the overall fraction of binaries that are circularized, while the top curves indicate the fraction of circularized binaries among those binaries that are very hard ($|E_{\text{bin}}| \gtrsim 1000kT$).

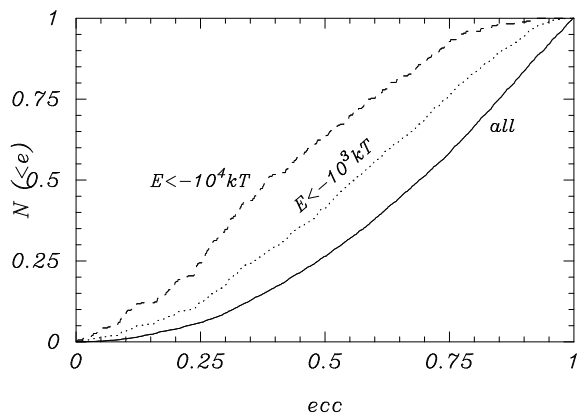


Figure 6. Cumulative distribution of the binary eccentricity. Solid line, initial conditions (the thermal distribution). The dashed and dotted line represent the eccentricity distributions at an age of 600 Myr of binaries with a binding energy $E_{\text{bin}} < -10^3 kT$ and $E_{\text{bin}} < -10^4 kT$, respectively. For the latter two curves the data for all models W4 and W6 are combined. However, we excluded those binaries which have been circularized by tidal forces.

transfer. While in many cases this type of evolution leads to a later shrinking of the orbit, in some rare cases the binaries remain wide after a period of modest mass transfer.

Since tidal forces drop off quickly with distance, in most cases they either succeed in fully circularizing a binary, or they do not cause much of an effect. Consequently, the eccentricity distribution of most non-circularized binaries changes little with time. Figure 6 illustrates this by presenting the cumulative distribution of all binaries with the exception of those with zero eccentricity. Note that this general argument does not hold for the hardest binaries: when we select only the hard ($|E_{\text{bin}}| \gtrsim 1000kT$) or super-hard ($|E_{\text{bin}}| \gtrsim 10^4 kT$) binaries, clear deviations from the initial thermal distribution are evident. This is not surprising: a $10^4 kT$ binary simply does not have enough room to develop an eccentricity of, say, 0.9, because the semimajor axis is too small.

3.3.2 Radial distribution of binaries

Figure 7 shows the binary fraction as function of distance to the cluster center at birth and at $t = 600$ Myr, adopted as a representative snapshot of an older cluster. (Qualitatively similar results would have been obtained had we selected any other time between ~ 200 Myr and 1 Gyr.) The upper solid line shows the initial distribution for all binaries, regardless of their binding energy. The lower solid line presents the initial fraction of binaries with a binding energy of at least $|E_{\text{bin}}| > 1000kT$. To avoid clutter, we have shown the statistical uncertainties in the form of error bars only for the bullet points; the uncertainties in the open and close triangles can be estimated by the scatter between neighboring points.

The triangles in Figure 7 shows the distribution for all binaries at $t = 600$ Myr for model W6 (open) and for model W4 (filled). The two distributions show similar trends, except for a generally smaller binary fraction in model W4 (see also Figure 5). The binary fraction in the central portion of the cluster is considerably higher than it was initially (upper solid line), because of mass segregation. For higher r values, the fraction of objects that are binary remains below the original value, all the way to and beyond the tidal radius.

The bullets indicate the distribution of binaries with $|E_{\text{bin}}| > 1000kT$ at a cluster age of 600 Myr. In order to improve our statistics, we have combined the data from the two models; the distributions are similar, with model W6 containing $\sim 8\%$ more hard binaries than model W4. Note that we find a higher proportion of hard binaries over the entire cluster field as compared to the initial distribution. This is mainly a result of dynamical evolution: hard binaries tend to get harder, and therefore some of the binaries contributing to the bullet points started off with a binding energy less than $1000kT$, and thus were not counted in the construction of the lower solid line.

The higher central concentration of very hard binaries, as compared to less hard binaries, is evident in Figure 8, which figure shows the cumulative distribution for single stars, hard $|E_{\text{bin}}| > 1000kT$ and super hard $|E_{\text{bin}}| > 10^5 kT$ binaries. The figure also presents the cumulative radial distribution for higher order (mostly triple) systems. The left-most and right-most dotted curves in Figure 8 show the radial distribution for model W6 at birth and at an age of 600 Myr, respectively. Initially, both single stars and binaries follow the left-most dotted curve. At an age of 600 Myr, all binaries are more centrally concentrated than the single stars (see the figure caption). The harder the binaries, the more centrally concentrated their distribution has become. In the case of triples, the condensation toward the center is extreme, with a triple half-mass radius of around 0.3 pc.

The high central concentration of the very hard $|E_{\text{bin}}| > 10^5 kT$ binaries is in part due to their early history. These binaries are largely the product of an unstable phase of mass transfer. The stellar components in these binaries were therefore more massive than they are at $t = 600$ Myr, so they are more strongly affected by mass segregation, causing them to sink to the central regions. In contrast, the moderately hard binaries with binding energies between $100kT$ and $10kT$ (not shown in Figure 8) are barely more centrally concentrated than the single stars. The triples are strongly centrally concentrated. This is the most dramatic result

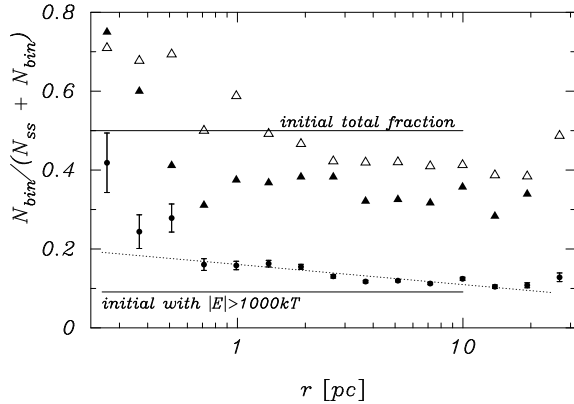


Figure 7. Fraction of binaries $N_{\text{bin}}/(N_{\text{ss}} + N_{\text{bin}})$ as function of the distance to the cluster center. The upper solid horizontal line shows the initial binary fraction over the entire star cluster. The cut off at about 10 pc is close to the location of the tidal radius. (Initially there were no stars beyond the tidal radius.) The lower solid curve presents the initial distribution for binaries with $|E_{\text{bin}}| > 1000kT$. The open triangles give the distribution of all binaries for model W6 at an age of 600 Myr. The solid triangles present the distribution of all binaries for model W4 at an age of 600 Myr. The bullets (with 1σ Poissonian error bars) present the fraction of hard $|E_{\text{bin}}| > 1000kT$ binaries as a function of the distance to the cluster center at an age of 600 Myr. These data combine models W4 and W6. To guide the eye we have placed a straight (dotted) line through these bullet points.

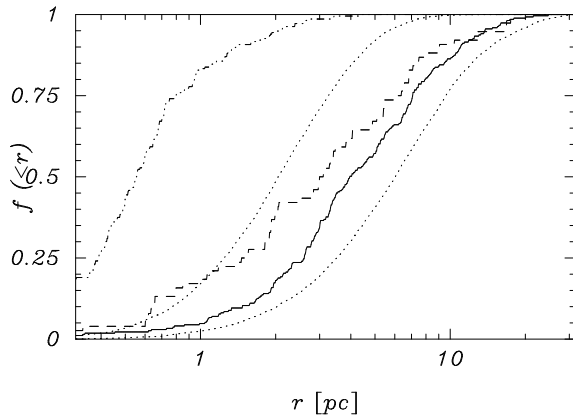


Figure 8. Cumulative radial distribution of single stars and binaries in models W4 and W6 (combined). The cumulative distribution for all single stars and binaries at birth and at $t = 600$ Myr are given by the left and right dotted curves, respectively. The solid curve gives the distribution for binaries with $|E_{\text{bin}}| > 10^3kT$ at an age of 600 Myr. The dashed curve gives the same distribution for $|E_{\text{bin}}| > 10^5kT$ binaries. The dash-3-dotted curve gives the radial distribution for higher order (mostly triple) systems. To improve statistics we accumulated all triples for models W4 and W6 over the time range of 550 Myr to 650 Myr.

of dynamical interactions: triple systems were not initially present, and must be created dynamically through encounters. Since the encounter rate increases sharply toward the cluster center, triples and higher-order systems are born, and often quickly destroyed again, near the very center of the cluster.

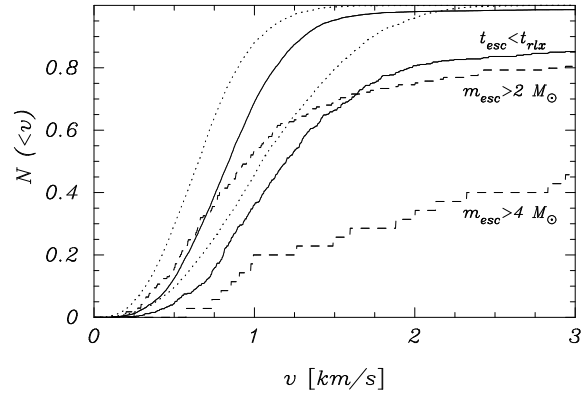


Figure 9. Cumulative distribution of the velocities of escaping single stars and binaries in models W4 and model W6 (combined). The two dotted lines show the velocity distributions of single stars in the models at zero age (right) and at $t = 600$ Myr (left). The left solid curve presents the distribution of the escaper velocity of all stars and binaries integrated over time. The right solid curve gives the velocity distribution of stars which escaped within the first half-mass relaxation time (~ 150 Myr). The two dashed curves give the escape speeds for stars with masses $m_{\text{esc}} > 2 M_{\odot}$ (upper) and $m_{\text{esc}} > 4 M_{\odot}$ (lower).

3.4 Escapers

The most important mechanism by which stars escape from the cluster is tidal stripping. Stars are assumed to have been tidally stripped once they reach two Jacobi (tidal) radii from the cluster center; they are then removed from the simulation. Stripped stars generally leave the cluster with relatively low velocities, as illustrated in Figure 9, which shows the distribution of escaper speeds for models W4 and W6.

It is convenient to draw a distinction between tidal evaporation and dynamical ejection of stars. Operationally, we distinguish between the two processes by the speed of the escaper; an “ejected” single star or binary leaves the cluster with a speed exceeding the escape velocity. That is, we infer the dynamics from the speed. Typically, this velocity is imparted to the escaping object during a strong interaction with another object in the cluster core. Because of the relatively low central densities (and hence low reaction rates) in our model clusters, this type of ejection is rather uncommon. White dwarf ejection velocities are not significantly different from those of main sequence stars, but giants have on average somewhat lower escaper velocities. This is mainly a consequence of the fact that giants are generally large and therefore cannot have very close encounters without colliding, so they are less able to pick up large escape velocities.

Another important escape mechanism is supernova explosions. A neutron star formed in a core-collapse supernova is hurled into space with a “kick” velocity that can easily exceed several hundreds of kilometers per second, greater than the cluster escape speed by 1–2 order of magnitude. These objects are hidden in the high-velocity tail of Figure 9; however, they are clearly visible in Figure 10 as the population of high-speed single objects with masses between $1 M_{\odot}$ and $2 M_{\odot}$.

A supernova in a binary system has several effects on the velocity distribution of both single and binary stars. The sudden mass loss in the supernova event, as well as

the asymmetric velocity kick, affect a binary’s internal orbital parameters and its center of mass velocity. When the binary is dissociated in the supernova, the companion to the exploding star is ejected with its orbital velocity, while the newly formed compact object receives an additional velocity kick. The effects of supernovæ on binary systems, and on the velocities of the binaries and single stars which result, are reviewed by Portegies Zwart (2000).

Figure 9 shows the velocity distribution of escaping stars and binaries from models W4 and W6. Due to the similarities in escape speeds between the two models, we have combined the data in a single plot. The escaper velocity distribution for single stars is slightly higher than that of the binaries. For clarity we show only the combined distribution of single and binary escapers in Figure 9. Escaper velocities are generally only slightly higher than the cluster velocity dispersion, and somewhat higher in the W4 models than in W6. The small fraction of high-velocity escapers in Figure 9 is due to neutron stars escaping after supernovæ explosions.

In addition to the overall escaper velocities for the combined models, Figure 9 also shows the distribution for stars which escaped within the first half-mass relaxation time (right solid line). This distribution has a considerably higher mean than the overall distribution. The figure also shows the velocity distributions for escaping stars more massive than $2M_{\odot}$ (top dashed curve) and $m_{\text{esc}} > 4M_{\odot}$ (lower dashed). These distributions are very different from the average escaper speed. Both models W4 and W6 experience high-density phases during their early evolution, within 1 initial half-mass relaxation time. The early escapers therefore have higher velocities. A similar process operates for the more massive escapers. The turn-off mass of a $2M_{\odot}$ star is about 800 Myr, while a $4M_{\odot}$ star lives for less than about 140 Myr. The distribution of escaper speeds for stars which escaped within t_{rlx} includes the stars with $m > 4M_{\odot}$. Still, the distributions are considerably different, in the sense that the massive stars have relatively high escape speeds. The reason for this discrepancy is the greater dynamical activity of the high-mass stars, which take part much more often in dynamical encounters with binaries.

The dependence of escaper velocity on escaper mass is illustrated in Figure 10. Most escapers have low masses and low velocities. The average escaper velocity in the W4 and W6 runs was 1.14 km s^{-1} and 1.00 km s^{-1} , respectively. Higher mass stars (and binaries) have considerably higher velocities. This trend was first observed by Blaauw (1961, see also Gies & Bolton 1986). Binaries are mostly ejected by dynamical encounters. Supernovæ are also responsible for numerous high velocity escapers, both from kicks and from binary effects, as mentioned above. The neutron stars are clearly visible in Figure 10 as the objects having masses of about $1.4M_{\odot}$ and velocities up to $\sim 1000 \text{ km s}^{-1}$.

Two rather low-mass ($m \sim 0.11M_{\odot}$ and $m \sim 0.7M_{\odot}$) stars have unusually large ($\sim 100 \text{ km s}^{-1}$ and 185 km s^{-1} , respectively) escape velocities. The more massive of the two was ejected from a tight binary at about $t = 5.6 \text{ Myr}$ when its companion exploded in a Type Ib supernova, dissociating the binary. The low-mass object was ejected following a three-body encounter at $t = 223 \text{ Myr}$.

Of all stars ejected from models W4 and W6, only 109 ($\sim 0.93\%$ out of a total of roughly 12,000) have velocities

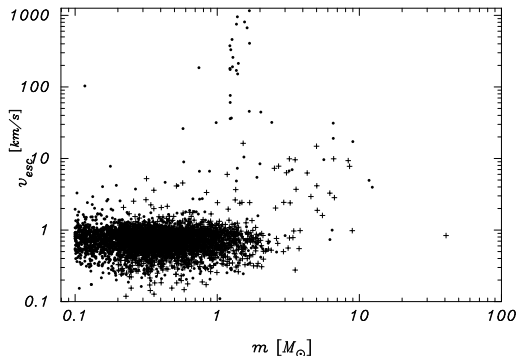


Figure 10. Mass versus velocity for escaping single stars (dots) and binaries (plus signs) in model W6. For the binaries, the total mass is used.

exceeding three times the dispersion velocity v_{disp} of the parent cluster. Of these, 46 are neutron stars. However, 57% of escapers with masses between $4M_{\odot}$ and $11M_{\odot}$, and 75% of escapers more massive than $11M_{\odot}$, have velocities more than $3v_{\text{disp}}$. The average escaper velocity of stars between $4M_{\odot}$ and $11M_{\odot}$ is 8.5 km s^{-1} ; stars with masses exceeding $11M_{\odot}$ have an average escaper velocity of 21 km s^{-1} , which is much higher than the cluster dispersion velocity.

These numbers are unusually high compared to the number of runaways in the Galactic disk. However, as our criterion here we have adopted three times the cluster velocity dispersion, instead of Blaauw’s (1961) criterion of 40 km s^{-1} (or three times the velocity dispersion in the Galactic disk). The fraction of high velocity stars following Blaauw (1961) was between $\sim 1\%$ for stars with $m \lesssim 11M_{\odot}$, about 2.5% for early B stars and about 20% among O stars ($m \gtrsim 16M_{\odot}$, see also Sone 1991). Among stars of spectral type A, Stone (1991) found a runaway frequency of $\lesssim 0.3\%$. These numbers are consistent with binary population synthesis studies of binaries in which stellar dynamical encounters are not taken into account (Portegies Zwart 2001).

The velocity dispersion of all stars in the cluster at an age of 600 Myr is $v_{\text{disp}} = 0.72 \pm 0.23 \text{ km s}^{-1}$. For stars within 1 pc (about the core radius) of the cluster center, $v_{\text{disp}} = 0.98 \pm 0.34 \text{ km s}^{-1}$; stars between 10 and 15 pc of the center have $v_{\text{disp}} = 0.59 \pm 0.16 \text{ km s}^{-1}$. Most striking is the higher velocity dispersion for stars well outside the tidal radius ($r > 15 \text{ pc}$) which have $v_{\text{disp}} = 0.75 \pm 0.20 \text{ km s}^{-1}$. A KS test indicates that the various velocity distributions are significantly different.

Drukier et al. (1998) reported a similar effect in the Globular cluster M15, and attributed it to tidal shocking. However, this process is not included in our models; we therefore conclude that the observed increase in the velocity dispersion outside the tidal radius cannot simply be a consequence of tidal shocks.

3.5 Collisions and Coalescence

Stellar mergers result from unstable mass transfer in a binary system or from direct collisions between stars. Some-

Table 4. Mergers occurring in models W4 and W6, compared with those in model calculations published previously. The first column identifies the two stars involved in the merger. The next two columns give the number of mergers in each model calculation, followed by the fraction of each merger type (expressed as a percentage, combining all runs). The last two columns give the fractions of mergers which occurred in models S of Papers I and II. Mergers between two remnants in Paper II (model S) are included here under {wd, wd}, although a few actually involved a neutron star or black hole.

Ntot:	W4	W6	total	Paper IS [%]	Paper IIS
{ms, ms}	92	110	84	77	80
{ms, gs}	19	11	12	14	6
{ms, wd}	0	1	0	5	11
{ms, ns}	1	0	0	1	1
{gs, ns}	0	0	0	3	0
{wd, wd}	5	0	2	0	2
{wd, ns}	0	2	1	0	0

times (unstable) mass transfer is initiated by the presence of a third star.

Table 4 gives an overview of the 241 collisions occurring during the model calculations discussed here. A schematic diagram of the relative frequencies of various collision configurations is presented in Figure 11. This figure may be compared directly with Figure 2 of Paper I, and with Figure 5 of Paper II. For easier comparison, we have added to Table 4 two columns summarizing the results of Papers I and II. Note, however, that the comparison with papers I and II is not really appropriate, as these model calculations lasted for 10 Gyr. According to a KS test there is no significant difference between the time histories of the collisions in the W4 and the W6 models.

Most ($\gtrsim 80\%$) mergers in models W4 and W6 occur between two main sequence stars (see Table 4). This was also the case in Papers I and II. In Paper I, however, only collisions between single stars were considered, and the high proportion of main-sequence collisions simply reflects the high proportion of main-sequence stars. Paper II included both collisions between single stars and mergers resulting from binary mass transfer, so the results in that case should compare better with models W4 and W6. The collisions reported in this paper, however, have a rather small contribution from {ms, wd} mergers compared to those in Papers I and II. This may be due in part to the smaller ages ($\lesssim 1$ Gyr) of our models compared with Papers I and II (< 10 Gyr).

Although clearly limited by small number statistics, an apparent difference between models W4 and W6 is the number of {wd, wd} mergers, which are much more common in model W4. This difference is reflected in the higher Type Ia supernova rate in model W4. Interestingly, the calculations in Paper II also had a high {wd, wd} merger fraction. In fact, if the binary population of models W4 and W6 were allowed to evolve after the disruption of the cluster, the rate of {wd, wd} mergers would be very similar to the results of Paper II. The cause of the high proportion of white-dwarf mergers in model W4 and Paper II is the larger amount of dynamical activity in these models, which drives more binaries into a state of mass transfer, favoring the formation

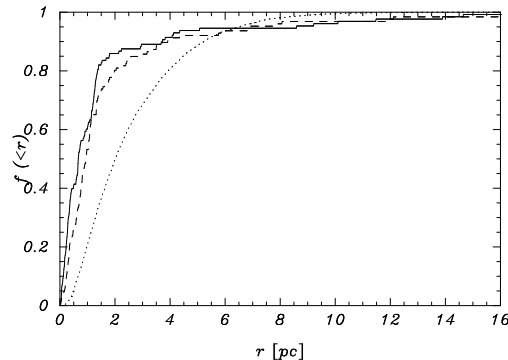


Figure 12. Cumulative distribution of the distance from the cluster center at which collisions occur in models W4 (dashes) and W6 (solid). The dotted line gives the initial distribution of stars in the W6 models.

of white-dwarf binaries (see also Hurley & Shara 2002). The resulting Type Ia supernova rate is discussed in the next section.

Figure 12 shows the radial distribution of collisions in models W4 and W6. More than 80% of all collisions occur within the initial half-mass radius (~ 3 pc). Collisions in the W6 models tend to be more concentrated to the cluster core than in the W4 models. It is striking that some ($\sim 5\%$) collisions occur far ($\gtrsim 8$ pc) from the cluster center. These collisions are induced by binary evolution, whereas mergers in the core are mainly caused by stellar encounters.

The expected distribution of masses and radii of colliding stars can be calculated following Portegies Zwart et al. (1997; see their Eq. 14). Assuming a Maxwellian velocity distribution with velocity dispersion v and including the effects of gravitational focusing, the number of collisions in the cluster per 10^8 year may be expressed as

$$\Gamma \approx \left(\frac{n}{10^3 \text{pc}^{-3}} \right)^2 \left(\frac{r_{\text{core}}}{\text{pc}} \right)^3 \left(\frac{m}{M_{\odot}} \right) \left(\frac{d}{R_{\odot}} \right) \left(\frac{\text{km s}^{-1}}{v} \right), \quad (1)$$

where m is the stellar mass. This rate is averaged over all other masses. (Note that, based on this estimate, we expect no collisions during the time span of our simulations for our adopted cluster parameters, underscoring the importance of binary interactions.)

Figure 13 shows the expected (upper panel; see paper III for details) and observed (lower panel) distributions of primary and secondary masses of stars involved in collisions in models W4 and W6. We excluded here the stars which merged as a result of unstable mass transfer. The upper panel is created via Eq. 1 from the initial mass function and the same mass-radius relation for zero-age main-sequence stars as was used in the model calculations. Gray shades indicate collision probability; darker shades correspond to higher values. The collisions observed in our models are presented in the lower panel. The masses of the colliding components in our model calculations are on average somewhat higher than expected. This phenomenon was first observed by Portegies Zwart et al. (1999; see also Portegies Zwart & McMillan 2002) in simulations of young star clusters having high central stellar densities. Portegies Zwart et al (1999)

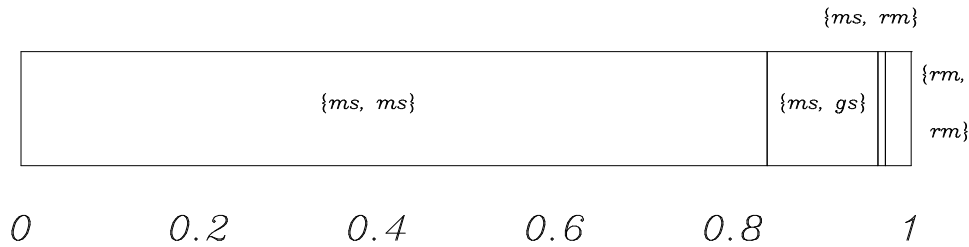


Figure 11. Schematic overview of the relative frequencies of mergers between various stellar types in models W4 and W6 (combined). Stellar types are denoted by *ms* for main sequence, *gs* for (sub)giants and *rm* for white dwarfs and neutron stars. Table 4 gives the numbers of occurrences.

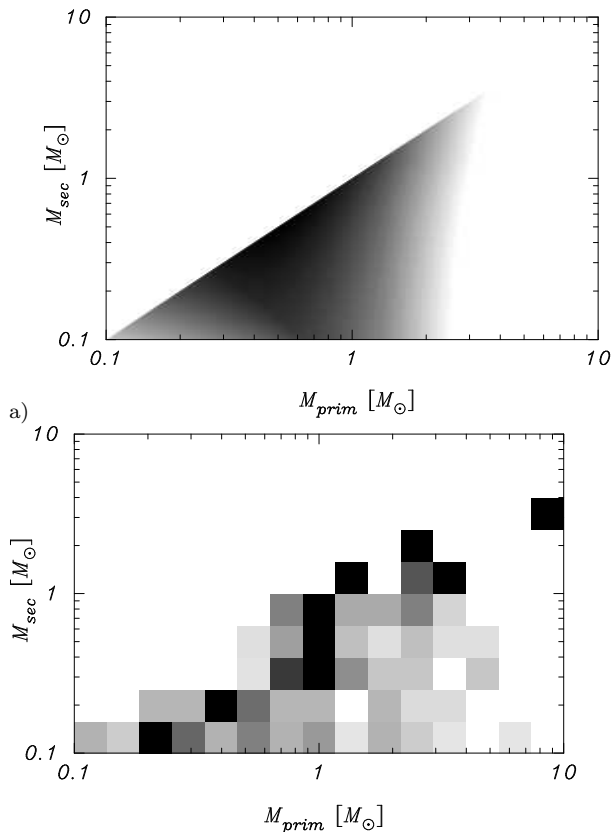


Figure 13. Relative collision rates between a primary and a secondary star as expected from Eq. 1 (upper panel), and as found in models W4 and W6 (lower panel). For the lower panel the mergers which resulted from an unstable phase of mass transfer are excluded; only the true collisions are taken into account. The shading is linear in the encounter probability in the upper panel and in the number of collisions in the lower panel. Darker shades indicate higher collision frequency. Since the probability distribution is symmetric about the line of equal masses, only the lower half of each figure is displayed.

used R136, a compact and very dense star cluster in the 30 Doradus region, as template for their simulations. We return to this comparison in the discussion section.

For 240 of the 241 stellar pairs experiencing a collision, we were able to reconstruct the orbit before the collision occurred. Figure 14 shows the orbital parameters for the bound

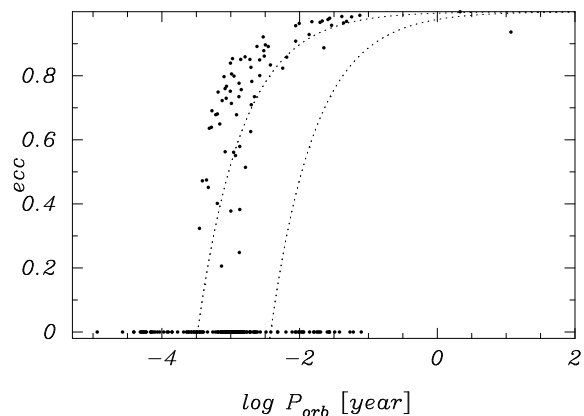


Figure 14. Orbital periods and eccentricities of coalescing binaries in models W4 and W6. Notice the rather large population of circular (zero eccentricity) binaries which experience a collision.

systems thus obtained. The single pair for which this reconstruction was not possible experienced a collision during a supernova event—the neutron star formed in the supernova was ejected directly into its $1.9 M_{\odot}$ main-sequence companion. In 181 of the 240 collisions ($\sim 71\%$), the orbit was circular on merger. The eccentricity distribution in the other bound cases is consistent with a thermal distribution. This result is consistent with the findings in Paper II, where for model *S*, 19% of the collisions were the result of a dynamical encounter.

3.6 Supernovae

Supernovae can dramatically affect the evolution of a star cluster. During a supernova, the exploding star ejects a large fraction of its mass at high speed. This mass quickly leaves the cluster, as the ejection velocity far exceeds the cluster’s escape speed. In addition, the newborn compact object may also receive a kick velocity large enough to escape the cluster. Binaries are very fragile to supernovae, and each binary hosting a supernova is likely to be dissociated.

3.6.1 Supernova types

Tables 5 and 6 present overviews of the supernovae observed in the models discussed in this paper, and compare them

Table 5. Observed supernova types (Obs, from Cappellaro et al. 1997) and supernovae occurring in a standard Scalo (1986) mass function (model IMF), the population synthesis calculations of model AK by Portegies Zwart & Verbunt (1996, model PZV-AK) and in models W4 and W6, and when the dynamical evolution of the stellar system is ignored (models W4-nd and W6-nd). The first column indicates the model, followed by the number of supernovae of types Ia, Ib, Ic and II. All numbers are normalized to 1.

model	Ia	Ib	Ic	II
Obs	0.09	0.11	0.18	0.62
IMF	—	—	0.12	0.88
PZV-AK	0.03	0.13	0.12	0.72
W4	0.22	0.20	0.07	0.50
W4-nd	0.06	0.20	0.17	0.57
W6	0.10	0.20	0.10	0.63
W6-nd	0.04	0.23	0.08	0.65

Table 6. Overview of the core-collapse supernovae which occurring in models W4 and W6. The progenitors are presented in the first column. When two stars are enclosed by parentheses, the left star explodes. Two stars enclosed by braces are the result of a merger or collision. The second column identifies the supernova type. Subsequent columns indicate how many core-collapse supernovae occurred in the models. The subdivisions *dyn* and *non-dyn* refer to models with and without dynamics. Superscript numbers indicate the numbers of binaries that survive the supernova. The rows below N_{esc} indicate the numbers of escapers experiencing a core collapse supernova *after* being ejected from the cluster. The table does not list the 3 stars in each model that collapse into black holes. The * indicates that one supernova occurred after a phase of mass transfer to a neutron star.

	Type	W4		W6	
	Type	dyn	non-dyn	dyn	non-dyn
Ntot:		38	35	25	26
wr	Ic	1	4 ²	0	2
gs	II	16	13	12	13
he	Ib	1	2	0	2 ¹
(gs, ms)	II	4	7	6	4
(gs, gs)	II	2	0	0	0
(gs, bh)	II	1	0	0	0
(he, ms)	Ic	3	2	2 ¹	0
(he, ms)	Ib	7 ¹	5	2	2 ¹
(he, he)	Ib	1	0	1	2
{wd, wd}	Ia	1	2	1	1
{gs, gs}	II	1	0	0	0
N_{esc}	total	16		6	
gs	II	2		1	
{wd, wd}	Ia	11		2	
(gs/he, ms)	Ib/II	2		3*	
{ms, ms}	II	1		0	

with expected supernova rates. Table 5 lists supernovae by type; Table 6 gives the evolutionary state of the exploding star and also indicates the possible presence of a binary companion. For comparison, we also present the expected number of supernovae given the same initial conditions, but ignoring the effects of dynamical evolution.

The adopted Scalo (1986) initial mass function contains

0.41 stars per thousand with $m > 25 M_{\odot}$ and 3.1 stars per thousand with $8 < m < 25 M_{\odot}$. In a naive evolution model, single stars with masses $\gtrsim 25 M_{\odot}$ may result in a Type Ic supernova, while stars more massive than $8 M_{\odot}$ produce a Type II supernova. For a population of 2000 single stars we then expect ~ 0.82 Type Ic and ~ 6.2 Type II supernovae. (Note that this estimate does not include binaries, and is therefore inapplicable to Type Ia and Ib supernovae.)

We compare these numbers with purely binary evolution models of Portegies Zwart & Verbunt (1996). According to their model AK, the Type Ic supernova rate is enhanced compared to models of only single stars. In the non-dynamical models (W4-nd and W6-nd), Type Ia and Ib supernovae occur without affecting the other supernova types. One reason for this is the fact that many Type Ib supernova originate from stars that were once part of a mass-transferring binary. The primary star in these binaries tends to lose its envelope in a phase of mass transfer and explode in a Type Ib supernova. The companion star, although initially not massive enough to experience a supernova, may accrete some material from the primary star. This accreted material may be sufficient to raise the secondary star’s mass over the limit for experiencing a supernova. Stellar mass is, in a sense, recycled to produce more supernovae (see also Portegies Zwart & Yungelson 1999).

The relative numbers of supernova types Ia:Ib/c:II for the 8 model clusters (models W4 and W6 combined) are 0.18:0.27:0.55; in the models where stellar dynamics is ignored these ratio are 0.05:0.34:0.61. The addition of dynamical interactions to the models enhances the Type Ia supernova rate at the expense of the Type Ib/c and Type II supernova rates. The enhancement of Type-Ib/c supernova in model W4 is due to close (post mass transfer) binaries, possibly because these binaries experience more dynamical encounters during the shallow collapse of the cluster core (see the discussion in §3.1).

3.6.2 Binary survival rate

Only two binaries survive their first supernova. One remains bound because the supernova results in a black hole, which does not receive a velocity kick. This binary experiences a second phase of mass transfer (see §3.7 for details). The other surviving binary is the result of a supernova in a rather short-period binary with a main-sequence companion. The resultant neutron star receives only a mild kick and the binary remains bound. Later this binary becomes an X-ray source (see §3.7 for details).

Two supernovae are triggered by collisions between carbon stars, resulting in Type Ia events, and one Type II supernova follows a collision between two supergiants. One neutron star is shot into its $1.9 M_{\odot}$ main sequence companion following a supernova. The resulting collision product, a Thorn-Zytkow star, is ejected from the star cluster before collapsing to a black hole.

Only two out of 29 binaries survive the formation of a neutron star and one survives the formation of a black hole. A total of six black holes result from type Ic supernovae.

Figure 15 gives the time history of the supernovae in models W4 and W6. First black holes (bullets) are formed, followed by neutron stars (circles, triangles and plus signs). The supernovae in the W4 models seem to occur somewhat

earlier than in the W6 models, but the mean time at which a supernova occurs, 23.3 Myr and 23.5 Myr for models W4 and W6, respectively, are not significantly different. The formation of a black hole at 46 Myr in model W6 is the result of a radio pulsar colliding with its carbon-star companion (see §3.7).

3.7 Mass transfer and peculiar binaries

3.7.1 First Roche-lobe contact

The high binary fractions in our models result in frequent episodes of mass transfer. This is illustrated in Figure 16, which shows the distribution of the times of first Roche-lobe contact in models W4 and W6. The various symbols indicate the state of the donor at the moment of first contact. (Note that helium stars, although likely to be the remnant of an earlier phase of mass transfer, are still counted in this figure.)

In most cases the mass is transferred to a main-sequence star, except in the cases indicated with \times , where the mass transfer is onto a compact object (mostly a white dwarf). In the majority of these latter cases the donor is a (sub)giant, but there are two occasions where the donor is a helium star, and in one case a main-sequence star (see Figure 17. One episode of mass transfer occurs between a (sub) giant and a black hole (model W4 at $t = 829$ Myr).

The time histories of models W4 are significantly different from those of models W6, according to a χ^2 test on the cumulative distributions of Figure 16. In the W4 models, mass transfer tends to occur earlier than in the W6 models. As discussed above, the difference is a result of the greater dynamical activity during the early phase of model W4. In fact, the higher binary activity in this case is caused by the early phase of shallow core collapse in the W4 models, which does not occur in the W6 models.

3.7.2 X-ray binaries

Mass transfer from a hydrogen- or helium-burning star onto a compact object generally leads to an X-ray phase. Figure 17 shows the distribution of orbital periods (in days) at the onset of Roche-lobe overflow for binaries with white-dwarf (in one case a black hole) accretor. Note the clear distinction between main-sequence and helium-star donors at short orbital periods and giant donors at larger periods. The wide systems with giant donors are probably most comparable to the supersoft sources (X-ray binaries where a white dwarf accretes at a super-Eddington rate for a solar-mass object, emitting at a rate of about 10^{38} erg/s).

A peculiar object which might be observable as an X-ray source results from a binary in which a helium giant ($2.5 M_{\odot}$) transfers mass to a $1.17 M_{\odot}$ carbon-oxygen white dwarf. First contact occurs at 45.9 Myr at an orbital period of 1.7 days. When the carbon star explodes and becomes a neutron star (at 46.07 Myr) it receives a kick of only 16 km s^{-1} . At that moment the companion star still fills its Roche lobe, and as a result the two stars coalesce into a single object. The merger product collapses a little later to form a $2.42 M_{\odot}$ black hole.

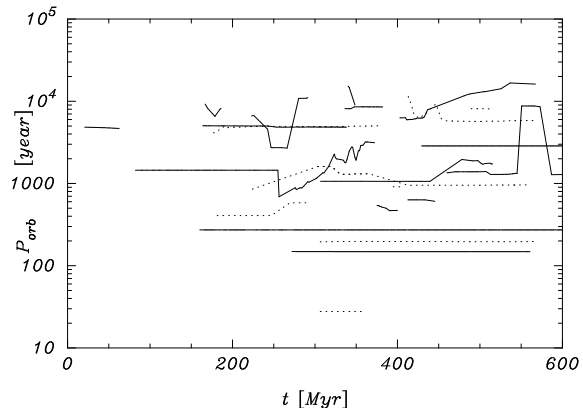


Figure 18. Orbital periods of the outer components of all hierarchical triples in all models, solid curves for the multiples in models W4, the dotted lines for the W6 multiples.

3.8 Triples and higher order systems

Long-lived triples and higher-order systems pose severe challenges to any numerical code. We encountered a total of 41 long-lived multiples in our runs, 21 triples [4 quadruples] in W4 and 13 triples [3 quadruples] in W6. Only one of the quadruple systems is hierarchical; the others are binary-binary systems.

The first multiple systems form as early as 20 Myr (by a binary-binary interaction); some survive for as long as 900 Myr. Figure 18 presents an overview of all triples in all models from $t = 0$ to 600 Myr. (At later times the numbers of triples decrease as the clusters dissolve.) The orbital period of the outer binary is generally rather constant. This is not surprising as, for the triple to be long-lived, it must be hierarchical and isolated, and the orbital energies and hence periods are adiabatic invariants. The systems showing a significant period derivative are driven by binary evolution or by temporary close encounters with other cluster members.

The fractions of long-lived triple and quadruple systems in our models are only $\sim 0.26\%$ and $\sim 0.12\%$, respectively, considerably smaller than the fraction of triples observed in the Galactic field (2.6%, Duquennoy & Mayor 1991) or in the Pleiades cluster ($\sim 2\%$, Mermilliod et al. 1990, 1992). Note also that these are the total numbers of multiple systems created at any time during our simulations. The mean lifetime of such a system is 280 ± 180 Myr.

We can study the population of short-lived multiple systems by selecting a bound pair of stars and searching for a third nearby star which forms a bound subsystem. At any moment in time the number of such short-lived multiple systems is about twice as high as the number of persistent triples. At $t = 600$ Myr we counted a total of 46 bound multiple systems in all models (W4 and W6), implying in a triple frequency of about 0.6% per star. For comparison, Kroupa (1995) found a triple fraction of 0.5% using a similar technique. The outer orbits of these triples, however, are generally rather soft.

Nine collision products in our models W4 became members of persistent triples or quadruples. These collisions occurred in transient triples. In about half (5) the cases, the two stars in the inner binary collided while the intruding star remained bound to the merged star. (For definiteness,

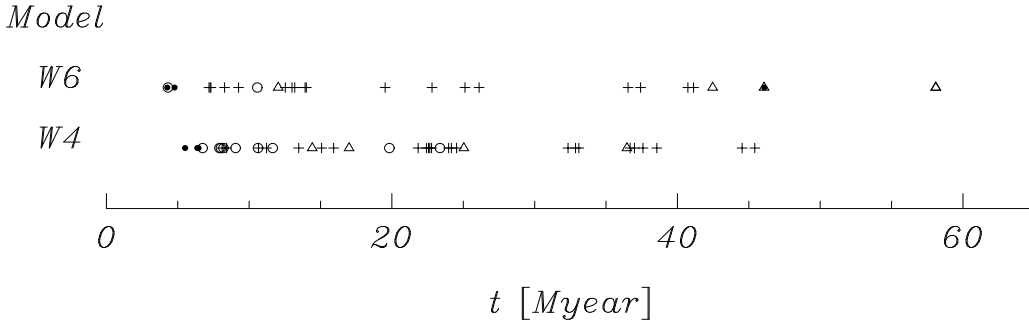


Figure 15. Supernova history for models W4 (bottom) and W6 (top). Type Ib, Ic and II supernovae are identified with circles, triangles, and plus-signs, respectively. Black-hole formation is identified with \bullet . Note the collapse of a neutron star to a black hole in one of the W6 models around $t \sim 46$ Myr (filled triangle). The time histories of these two distributions are not significantly different.

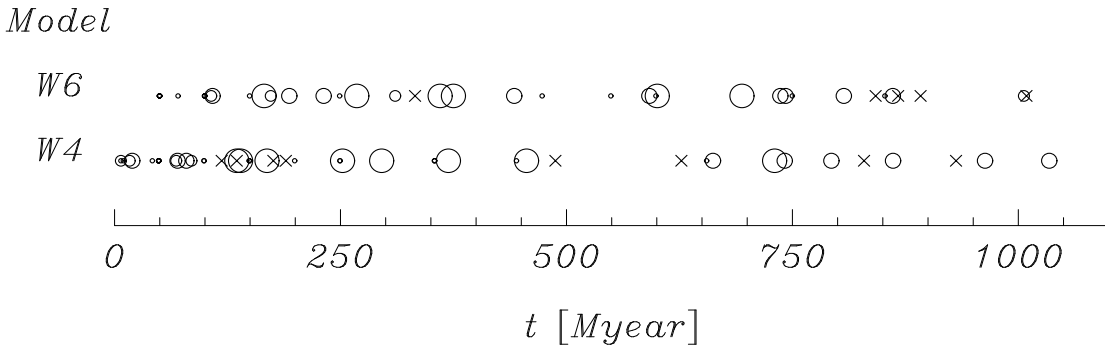


Figure 16. Times of first mass transfer for binaries in models W4 and W6. The circle size indicates the evolutionary state of the donor, from main-sequence (small) via Hertzsprung gap, and sub-giant, with supergiant indicated by the largest circles. The \times symbols indicate mass transfer onto a white dwarf (or a black hole, for the second \times from the right in model W4).

we take the “inner” orbit in a quadruple system to be the larger of the two inner orbits.) In a few cases (3), the merger product and its companion became bound to another third star, forming a stable triple. In two of these cases, the encounter resulted in second collision with the merger product. Both these triple collisions resulted in blue stragglers which had, at some time, a mass exceeding twice the turnoff mass of the cluster.

Of the total of 117 collisions in the W4 models, nine occurred in transient triple systems. With a triple frequency of only $\sim 0.26\%$, one naively expects less than one collision to occur in triples, making the frequency of collisions in triples unusually high. In part, this higher fraction of collisions in multiples is due to the dynamics—such systems generally form close to the cluster center, where the stellar density is highest and most collisions are expected. In addition, collision products tend to be found near the center, because they are more massive than average. The higher combined mass of three stars and the relatively large cross section of the outer orbit also increases the collision probability. Similar circumstances led to the high collision rates observed in the R 136 simulations of Portegies Zwart et al. (1999, see also Portegies Zwart & McMillan 2002). Thus, triples are favorable for collisions, and collision products favor triple systems.

We can characterize the triple systems formed in our simulations as follows: All inner orbits have periods less than

100 year with an average of about 5.1 years. All outer orbital periods exceed 100 year and have an average of about 4600 years. The eccentricities of the inner and outer orbits are quite distinct. The inner orbits have generally rather small eccentricities ($e = 0.44 \pm 0.3$) and its distribution is consistent at a 98.8% level with the inner eccentricity distribution of observed triples (Tokovinin 1997). The distribution of outer eccentricities ($e = 0.65 \pm 0.14$) is consistent with thermal.

4 COMPARISON WITH PREVIOUS WORK

4.1 McMillan & Hut 1994

The simulations reported by McMillan and Hut (1994) used up to 2048 stars, with up to 20% (rather soft: $1 - 20$ or $1 - 100kT$) primordial binaries, and included the Galactic tidal field. However, they excluded stellar evolution and hence any stellar mass loss. In the absence of a physical time scale associated with stellar evolution, they presented their results in units of the initial relaxation time. Our W6 models have half lives of about 6 initial relaxation times, much shorter than the $\sim 12-30$ initial relaxation times for the most comparable McMillan & Hut models. Stellar mass loss is the main reason for the more rapid dissolution of our models; in addition, the McMillan & Hut runs all began with the cluster well inside its Jacobi surface, so the clusters had to expand significantly before significant tidal mass loss

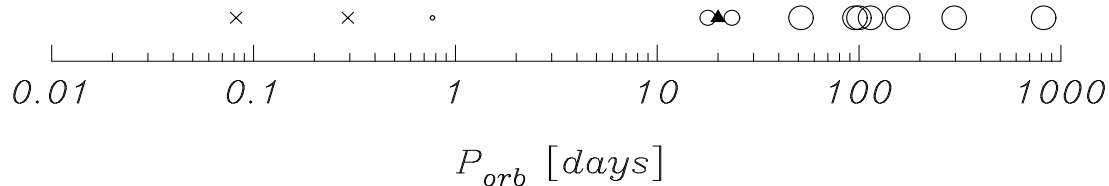


Figure 17. Orbital period (in days) at the onset of mass transfer onto a compact object, for models W4 and W6. The circle size indicate the evolutionary state of the donor, from main sequence (smallest circles) to supergiant (large circles). The \times indicates that the donor is a helium star; the filled triangle indicates the period of the single black hole X-ray binary.

occurred. As discussed previously, all the McMillan & Hut models experienced core collapse, which is not seen in our simulations, where core collapse is arrested by stellar mass loss.

McMillan & Hut found that the binary fraction in their simulations first fell due to as binaries were destroyed by interactions with other binaries in the cluster core, then rose again at late times as the cluster evaporated in the Galactic tidal field. In contrast, we find that the (initially $\sim 50\%$) binary fraction in our models remains roughly constant throughout the calculation, then increases significantly to $\sim 70\%$ when only $\sim 10\%$ of the cluster mass remains. These differences are most likely attributable to the lack of significant core collapse and the stronger tidal fields in our runs.

One of the most interesting conclusions made by McMillan & Hut is that the spatial distribution of hard binaries is different than the distribution of soft binaries (see their Figure 9). In Figure 7 we showed that hard binaries ($E > 1000kT$) are slightly more centrally concentrated than average.

4.2 Kroupa 1995

The main difference between our calculations and those of Kroupa (1995) is his neglect of binary evolution and his inclusion of a prescription for pre-main-sequence binaries. The eccentricity distribution of his 'primordial' binaries was therefore somewhat different from ours, but this affects only binaries with the highest eccentricities and the shortest orbital periods. On the other hand, his neglect of binary evolution underestimated the fraction of tidally circularized binaries. In his calculations the boundary between hard and soft binaries was at an orbital period of roughly 2.7×10^4 years, similar to that in our models W4. We have already compared the characteristics of the populations of triple systems in our calculations (see §3.8).

4.3 De La Fuente Marcos 1997

De la Fuente Marcos (1997) performed studies of the evolution of small ($N \leq 750$), tidally limited open clusters having a variety of initial mass functions, with and without the inclusion of stellar (but not binary) evolution. All models started with a substantial fraction (1/3) of primordial binaries having mass ratios of 0.5 and energies in the $\sim 1\text{--}10kT$ range. He found that the dissolution time scale of his models depended quite sensitively on the choice of IMF, and that the binary population shortly before dissolution could

show characteristic features allowing remnants of rich and poor clusters to be distinguished observationally. It is unclear how these results extend to larger systems.

The binary fraction in the de la Fuente Marcos simulations ranged from 33% initially to about $51\% \pm 0.19\%$ near the disruption of the cluster (averaged over all 20 of his simulations). By the time the clusters dissolved, the binary fraction in the core had dropped to $15\% \pm 0.13\%$. We find a similar increase in the total binary fraction, but clearly the core binary fraction in our models is much higher (see Figure 7). The small binary fractions in the core near the end of his simulations are the direct result of his choice of initial binary binding energies.

4.4 Papers I, II

The comparison between the relative collision frequencies in Tab. 4 and those of model *S* in Paper I are quite striking. In that paper only encounters between single stars were studied and primordial binaries were neglected. Still, in Paper I 77% of all collisions occurred between two main-sequence stars, and 14% between a main-sequence star and a giant; the remaining 9% involved giants and remnants.

The (ms, ms) merger rates in our models are comparable to the merger rates in paper II, but (ms, wd) were much greater in model *S* of paper II because it is older (10Gyr). The (ms, gs) merger rate is lower because there are fractionally fewer main-sequence stars in paper II.

4.5 Hurley et al. 2001

Hurley et al. (2001) have modeled the open cluster M67, using a simulation code similar in many ways to our own. Both codes use fitting formulae for single star evolution, and include a series of recipes for dealing with binary star evolution. The main difference between Hurley et al. (2001) and the current paper lies in the parameter choices for their simulations: they evolved 15,000 stars to an age of 2500 Myr, before adding dynamics, in the form of a direct N -body calculation. They then evolved the combined model to an age of 4300 Myr, appropriate for the old open cluster M67. They also present the results from smaller N -body runs, starting at earlier times.

Hurley et al. (2001) focused mostly on the formation of blue stragglers, and reported that their simulations indeed produced roughly the right number of blue stragglers, in agreement with observations of M67. They also performed a non-dynamical binary evolution population synthesis, and found that the number of blue stragglers in that case fell

short of that required by observations. They concluded that dynamical encounters have been crucial in the evolution of M67. While it is difficult to make a quantitative comparison between their simulations and ours, given the rather different types of initial conditions, our main results concerning the numbers and types of collisions, and the formation rate of triples are in broad agreement.

5 SUMMARY AND CONCLUSIONS

We have performed detailed N -body calculations of intermediate-mass open clusters near the Sun. The initial conditions were selected to mimic star clusters such as Pleiades, Praesepe and Hyades. Our calculations included the effects of dynamical encounters between stars and higher order systems, the tidal field of the parent Galaxy and the evolution of single stars and binary stars.

5.1 Cluster lifetime and structure

Our model star clusters dissolved in the tidal field of the Galaxy within about 1 billion years. The rate of mass loss remained roughly constant, at ~ 0.8 – $1.4 M_{\odot}$ per million years, corresponding to a cluster half-life of ~ 600 – 1000 Myr, depending on distance from the Galactic center.

The density profiles of the model clusters changed dramatically during the cluster lifetime. Core collapse was prevented by stellar mass loss and binary heating. Our less concentrated (W4) models became more compact during the first few million years, whereas the more concentrated (W6) models expanded from the beginning. The W4 models still dissolved more quickly in the Galactic tidal field, however, mainly due to their closer proximity of the Galactic center.

Mass segregation is a very efficient process. After only a small fraction of an initial relaxation time, single white dwarfs, giants, collision products, hard binaries, mass transferring binaries and binaries with one or two massive components (compared to the mean mass in the cluster) were all noticeably more centrally concentrated than the average star, as measured by the half mass radii of the various components.

5.2 Binary stars

The numbers of binaries decreased with time at roughly the same rate as the numbers of single stars, with the result that the binary fractions in our models remained more or less constant over the studied range of cluster ages. The binary fraction generally decreased during the first few million years by several percent, due to supernovae and dynamical encounters, both of which tended to disrupt binaries. For the remainder of the evolution, this fraction slowly increased. The maximum binary fraction of $\sim 65\%$ is reached near disruption. The fraction of binaries in the core remained between 50% and 60% higher than the fraction near the half-mass radius over the entire lifetime of the cluster.

The widest binaries were dissociated soon after the start of the simulations. A considerable fraction ($4.5 \pm 0.6\%$) of highly eccentric binaries with rather short orbital periods circularized and some experienced mass transfer early in the evolution of the cluster. These short-period binaries were

generally more centrally concentrated than wider binaries or single stars, because they are on average more massive than single stars and do not interact.

The overall distributions of binary parameters, however, hardly change with time. Apart from the loss of binaries with the largest orbital periods and those with short orbital periods and high eccentricities, most binaries were relatively unaffected by either stellar evolution or stellar dynamics. The observed binary populations in open clusters may therefore be a reasonable representation of the initial primordial population.

5.3 Escapers

We define three families of escaping stars. (1) Neutron stars were ejected from the cluster with very high velocities. About 0.4% of all stars were ejected as neutron stars due to supernova explosions. (2) Massive stars tended to have rather high escape velocities, because they were often found in close binaries which were disrupted by the explosion of the primary star, possibly after a phase of mass transfer. The average escape velocity of all single main sequence stars in model W4 was $v_{\text{esc}} = 1.2 \pm 0.51 \text{ km s}^{-1}$, whereas stars with $m \gtrsim 4 M_{\odot}$ had $v_{\text{esc}} = 17.4 \pm 2.3 \text{ km s}^{-1}$. For model W6 these numbers are only slightly smaller. (3) The mean escaper velocity of low-mass stars ($v_{\text{esc}} = 1.0 \pm 0.28 \text{ km s}^{-1}$ for stars with $m < 0.5 M_{\odot}$) was comparable to the cluster velocity distribution; the mean velocity of escaping binaries was ($v_{\text{esc}} = 0.97 \pm 0.29 \text{ km s}^{-1}$ for model W4 and $v_{\text{esc}} = 0.81 \pm 0.29 \text{ km s}^{-1}$ for model W6), somewhat smaller than that for single stars.

5.4 Stellar collisions

Not surprisingly, collisions tended to occur near the cluster center, but a considerable fraction of mergers occurred farther out, near the tidal radius. More than 80% of all collisions occurred within about two core radii. Most ($\sim 80\%$) collisions occurred between two main sequence stars. About 70% of the collisions were the result of an unstable phase of mass transfer. The rest occurred in single-star–binary or binary–binary encounters. Multiple collisions were rare: only two out of 241 in our model calculations.

Collision participants were somewhat more massive than expected based on the simple cross section arguments presented in Paper III. Most (85%) collisions occurred between main-sequence stars; most of the remainder involved a main-sequence star and a giant (12%). Only 3% of the collisions occurred between two remnants. The dynamical activity in the cluster core, however, caused quite a few white dwarfs to become binary members, which would later merge due to the emission of gravitational waves. This leads to a rather high merger rate among white dwarfs (see also Shara & Hurley 2002).

5.5 Supernovae and stellar remnants

The overall supernova rate in our simulations was consistent with rates observed in the Galaxy. However, the ratios of Type II to Type Ia, Ib, and Ic supernova are quite different. Most striking is the order of magnitude enhancement

of type Ia supernovae in the W4 models compared to the non-dynamical models and the population synthesis of non-interacting binaries. In these same models, Type Ib supernova are enhanced by about a factor of two compared to a population of binaries without dynamical encounters.

Because of the assumed neutron-star kick distribution, pulsars were generally not retained in our cluster models. Only one out of 61 neutron stars was retained to form an X-ray binary later in its lifetime. The observed velocity distribution of ejected pulsars was somewhat smaller than the input kick velocity distribution. X-ray binaries in which a white dwarf accretes from a companion star were about an order of magnitude more common. X-ray binaries containing black holes were rare simply because such objects form from the highest-mass stars, which are themselves rare.

Among the more unusual collisions, in our simulations, we observed one between a neutron star and a helium giant, two between CO white dwarfs, resulting in type Ia supernovae and the formation of an X-ray binary with a black hole as accretor. Several white dwarfs experienced a phase of mass transfer from a companion star. The donor was most often a (sub)giant. In total, 13 X-ray binaries were formed, most with a white dwarf as accretor.

5.6 Multiple systems

The number of persistent triples formed in our calculations was about an order of magnitude smaller than the observed fraction of triples in open clusters and the Galactic disk, although the frequency of triples and higher-order systems present at any moment in our simulations was comparable to the numbers actually observed. The majority of these were transient, however, and their orbital parameters differed considerably from observations. The orbital parameters of the outer orbits of the formed triples formed in our models was not representative of triples observed in the Galaxy, which tend to have shorter periods and lower eccentricities.

ACKNOWLEDGMENTS

This work was supported by NASA through Hubble Fellowship grant HF-01112.01-98A (NASA contract NAS 5-26555) by the Space Telescope Science Institute, the Royal Netherlands Academy of Sciences (KNAW), the Netherlands organization for scientific research (NWO), by NASA ATP grants NAG5-6964 and NAG5-9264. Calculations were performed on the GRAPE-4 systems at Tokyo University, Drexel University and the University of Bloomington. SPZ is grateful to Drexel University, Tokyo University and the Institute for Advanced study for their hospitality.

REFERENCES

Abt, H. A., Levy, S. G. 1972, *ApJ*, 172, 355
 Andrievsky, S. . M. 1998, *A&A*, 334, 139
 Blaauw, A. 1961, *ban*, 15, 265
 Bouvier, J., Rigaut, F., Nadeau, D. 1997, *A&A*, 323, 139

Cappellaro, E., Turatto, M., Tsvetkov, D. Y., Bartunov, O. S., Pollas, C., Evans, R., Hamuy, M., 1997, *A&A*, 322, 431
 Cox, A. N. 1954, *ApJ*, 119, 188
 Dachs, J., Kabus, H. 1989, *A&As*, 78, 25
 de la Fuente Marcos, R., 1997, *A&A*, 322, 764
 Drukier, G. A., Slavin, S. D., Cohn, H. N., Lugger, P. M., Berrington, R. C., Murphy, B. W., Seitzer, P. O. 1998, *AJ*, 115, 708
 Duquennoy, A., Mayor, M. 1991, *A&A*, 248, 485
 Frandsen, S., Dreyer, P., Kjeldsen, H. 1989, *A&A*, 215, 287
 Gies, D. R., Bolton, C. T. 1982, *ApJ*, 260, 240
 Harris, G. L. H., Fitzgerald, M. P. V., Mehta, S., Reed, B. C. 1993, *AJ*, 106, 1533
 Hartman, J. W. 1997, *A&A*, 322, 127
 Hartwick, F. D. A., Hesser, J. E. 1971, *PASP*, 83, 53
 Hawley, S. L., Tourtellot, J. G., Reid, I. N. 1999, *AJ*, 117, 1341
 Heggie, D. C., Ramamani, N. 1995, *MNRAS*, 272, 317
 Hodgkin, S. T., Pinfield, D. J., Jameson, R. F., Steele, I. A., Cossburn, M. R., Hambly, N. C. 1999, *MNRAS*, 310, 87
 Hurley, J. R., Tout, C. A., Aarseth, S. J., Pols, O. R. 2001, *MNRAS*, 323, 630
 Hurley, J. R., Tout, C. A., Pols, O. R. 2002, *MNRAS*, 329, 897
 Ianna, P. A., Adler, D. S., Faudree, E. F. 1987, *AJ*, 93, 347
 Jones, B. F., Stauffer, J. R. 1991, *AJ*, 102, 1080
 King, I.R., 1966, *AJ*, 71, 64
 Kroupa, P. 1995, *MNRAS*, 277, 1522
 Makino, J. 1991, *ApJ*, 369, 200
 Makino, J., Aarseth, S. J. 1992, *PASJ*, 44, 141
 Makino, J., Taiji, M., Ebisuzaki, T., Sugimoto, D. 1997, *ApJ*, 480, 432
 McMillan, S., Hut, P., Makino, J. 1990, *ApJ*, 362, 522
 McMillan, S., Hut, P., Makino, J. 1991, *ApJ*, 372, 111
 McMillan, S., Hut, P. 1994, *ApJ*, 427, 793
 McMillan, S. L. W. 1986a, *ApJ*, 306, 552
 McMillan, S. L. W. 1986b, *ApJ*, 307, 126
 McMillan, S. L. W., Hut, P. 1996, *ApJ*, 467, 348
 Mermilliod, J. C., Mayor, M. 1999, in 10 pages, 3 tables, 7 eps figures. Accepted for *A&A*; LaTeX Preprint no. IAUL preprint no 85., 11405
 Mermilliod, J. C., Rosvick, J. M., Duquennoy, A., Mayor, M. 1992, *A&A*, 265, 513
 Mermilliod, J. C., Weis, E. W., Duquennoy, A., Mayor, M. 1990, *A&A*, 235, 114
 Nordstroem, B., Andersen, J., Andersen, M. I. 1996, *A&As*, 118, 407
 Nordstroem, B., Andersen, J., Andersen, M. I. 1997, *A&A*, 322, 460
 Perryman, M. A. C., Brown, A. G. A., Lebreton, Y., Gomez, A., Turon, C., De Strobel, G. C., Mermilliod, J. C., Robichon, N., Kovalevsky, J., Crifo, F. 1998, *A&A*, 331, 81
 Pinfield, D. J., Jameson, R. F., Hodgkin, S. T. 1998, *MNRAS*, 299, 955
 Portegies Zwart, S. F. 2000, in *ApJ* in press., 5202
 Portegies Zwart, S. F., Hut, P., Makino, J., McMillan, S. L. W. 1998, *A&A*, 337, 363
 Portegies Zwart, S. F., Hut, P., Verbunt, F. 1997, *A&A*, 328, 130
 Portegies Zwart, S. F., Makino, J., McMillan, S. L. W., Hut, P. 1999, *A&A*, 348, 117

- Portegies Zwart, S. F., Makino, J., McMillan, S. L. W., Hut, P. 2001, *ApJl*, 546, L101
- Portegies Zwart, S. F., McMillan, S. L. W. 2002, *ApJ*, 576, 899
- Portegies Zwart, S. F., van den Heuvel, E. P. J. 1999, *New Astronomy*, 4, 355
- Portegies Zwart, S. F., Verbunt, F. 1996, *A&A*, 309, 179
- Portegies Zwart, S. F., Yungelson, L. R. 1998, *A&A*, 332, 173
- Portegies Zwart, S. F., Yungelson, L. R. 1999, *MNRAS*, 309, 26
- Raboud, D., Mermilliod, J. C. 1998, *A&A*, 329, 101
- Reid, I. N., Hawley, S. L. 1999, *AJ*, 117, 343
- Sandrelli, S., Bragaglia, A., Tosi, M., Marconi, G. 1999, *MNRAS*, 309, 739
- Scalo, J. M. 1986, *Fund. of Cosm. Phys.*, 11, 1
- Shara, M. M., Hurley, J. R. 2002, *ApJ*, 571, 830
- Stone, R. C. 1991, *AJ*, 102, 333
- Tokovinin, A. A. 1997, *A&As*, 124, 75
- van Den Hoek, L. B., de Jong, T. 1997, *A&A*, 318, 231

This paper has been typeset from a $\text{\TeX}/\text{\LaTeX}$ file prepared by the author.

Star cluster ecology V: Dissection of an open star cluster—spectroscopy

Simon F. Portegies Zwart,^{1*} Piet Hut,² Stephen L. W. McMillan³ and Junichiro Makino,⁴

¹ *Astronomical Institute 'Anton Pannekoek', University of Amsterdam, Kruislaan 403, 1098SJ Amsterdam, the Netherlands, Section Computational Science, University of Amsterdam, Kruislaan 403, 1098SJ Amsterdam, the Netherlands*

² *Institute for Advanced Study, Princeton, NJ 08540, USA*

³ *Department of Physics, Drexel University, Philadelphia, PA 19104, USA*

⁴ *Department of Information Science and Graphics, College of Arts and Science, University of Tokyo, 3-8-1 Komaba, Meguro-ku, Tokyo 153, Japan*

Accepted 2145 December 32. Received 1687 December -1; in original form 1900 October 11

ABSTRACT

We have modeled in detail the evolution of rich open star clusters such as the Pleiades, Praesepe and Hyades, using simulations that include stellar dynamics as well as the effects of stellar evolution. The dynamics is modeled via direct N -body integration, while the evolution of single stars and binaries is followed through the use of fitting formulae and recipes. The feedback of stellar and binary evolution on the dynamical evolution of the stellar system is taken into account self-consistently.

Our model clusters dissolve in the tidal field of the Galaxy in a time span on the order of a billion years. The rate of mass loss is rather constant, $1 \sim 2 M_{\odot}$ per million years. The binary fraction at first is nearly constant in time, then increases slowly near the end of a cluster's lifetime. For clusters which are more than about 10^8 years old the fractions of stars in the form of binaries, giants and collision products in the inner few core radii are considerably higher than in the outer regions, beyond the cluster's half mass radius. When stars with masses $\gtrsim 2 M_{\odot}$ escape from the cluster, they tend to do so with velocities higher than average.

The stellar merger rate in our models is roughly one per 30 million years. Most mergers are the result of unstable mass transfer in close binaries ($\sim 70\%$), but a significant minority are caused by direct encounters between single and binary stars. While most collisions occur within the cluster core, even beyond the half mass radius collisions occasionally take place. We notice a significant birthrate of X-ray binaries, most containing a white dwarf as the donor. We also find some X-ray binaries with a neutron-star donor, but they are relatively rare. The persistent triple and higher order systems formed in our models by dynamical encounters between binaries and single stars are not representative for the multiple systems observed in the Galactic disk or in open clusters. We conclude that the majority of multiples in the disk probably formed when the stars were born, rather than through later dynamical interactions.

Key words: Methods: N-body simulations – Binaries: general – Binaries: close – Open cluster and associations: general – Open cluster and associations: NGC2516, NGC2287, Praesepe, Hyades, NGC 2660, NGC 3680

1 INTRODUCTION

Open clusters are useful laboratories for studying the interplay between single star evolution, binary star evolution and stellar dynamics. Unlike their bigger (and older) siblings, the globular clusters, they contain a manageable number of stars, and the evolution of the majority of the stars is not expected to be strongly affected by the dynamics. Still, a

significant number of collisions and subsequent stellar mergers can take place, as well as dynamically induced exchange reactions between single stars and binaries. For all these reasons, the usual zoo of objects created in binary stellar evolution is significantly enlarged by the presence of even more exotic specimens that could not have formed *in vitro* through isolated evolution, but only *in vivo* through the dynamical interplay of initially unrelated (single or multiple) stars.

* E-mail: spz@science.uva.nl; KNAW fellow

The simulations reported here have been run on a

Table 1. Observed and derived parameters for several open star clusters with which our simulations may be compared. References to the literature (second column) are: (a) Pinfield et al. (1998); Raboud & Mermilliod, (1998); Bouvier et al (1998); (b) Abt & Levy (1972); Dachs, J & Kabus (1989); Hawley et al. (1999). (c) Harris et al. (1993); Ianna et al (1987); Cox (1954). (d) Andrievsky (1998); Jones & Stauffer (1991); Mermilliod & Mayor (1999); Mermilliod et al. (1990); Hodgkin et al. (1999). (e) Perryman et al. (1998 and references therein) Reid & Hawley (1999); (f) Frandsen et al. (1989); Hartwick & Hesser (1971); Sandrelli et al. (1999). (g) Hawley et al. 1999 ; Nordström et al. (1997); Nordström et al. (1996). Subsequent columns give (3) the distance to the cluster (in pc), (4) the cluster age (in Myr), (5) the half mass relaxation time, (6) the crossing time, (7) the total mass (in M_{\odot}), (8) estimate for the half mass radius (in pc), and (9) the core radius. In cases where the relaxation time is not given in the literature, we calculate it (see Paper IV); these entries are indicated by *. The final two columns contain information about cluster stellar content. The column labeled $f_{s:b:t}$ indicates the number of single stars, binaries and triples (separated by colons). For clusters where the numbers are given directly by observations, the table gives the observed numbers of each system. If the binary fraction is derived by other methods, we give the relative fractions normalized to the number of single stars. The last column ($N_{\text{bss:Be:gs}}$) gives the number of observe blue stragglers, Be stars and giants, separated by a column.

name	ref.	d [pc]	t — [Myr] —	t_{rlx} (5)	t_{hm} (6)	M [M_{\odot}] (7)	r_{tide} (8)	r_{hm} — [pc] — (9)	r_{core} (10)	$f_{s:b:t}$ (11)	$N_{\text{bss:Be:gs}}$ (12)
(1)	(2)	(3)	(4)	(5)	(6)	(7)	(8)	(9)	(10)	(11)	(12)
Pleiades	a	135	115	150	8	~ 1500	16	2–4	1.4	137:60:2	3:3:?
NGC2516	b	373	110	220		1000		2.9		16:6:?	6:3:4
NGC2287	c	675	160–200	—			6.3			1:0.6:?	3:1:8
Praesepe	d	174	400–900	220		1160		12	2.8	1:0.3:0.03	?:5:?
Hyades	e	46	625	320	15	1027	10.3	3.7 ¹	2.6	1:0.4:0	1:0:4
NGC 2660	f	2884	900–1200	260		400	?	4	~ 1	0:0.3:?	18:4:39
NGC 3680	g	735	1450	28		100	4.3	1.2	~ 1	44:25:0	4:4:17

Table 2. Initial conditions and parameters for the selected models. The first column gives the model name, followed by the cluster mass (in M_{\odot}), the King (1966) parameter W_0 , the distance to the Galactic center (in kpc), the initial relaxation time and half mass crossing time (both in Myr). The remaining columns give the location of the cluster’s Jacobi surface along the $X-$ (towards the Galactic center), $Y-$ and $Z-$ (towards the Galactic pole) axes, and the initial virial radius, half mass radius and core radius (all in parsec).

name	M [M_{\odot}]	W_0	R_{Gal} [kpc]	t_{rlx} [Myr]	t_{hm}	r_{Jacob} [pc]	r_{vir}	r_{hm} [pc]	r_{core}		
W4	1708	4	6.8	135	4.07	14.5	9.7	7.2	2.5	2.14	0.83
W6	1603	6	10.4	140	4.15	21.6	14.4	10.8	2.5	2.00	0.59

GRAPE-4 (Makino et al. 1997) system, a special-purpose computer designed to speed up stellar-dynamical calculations. While the models in this paper contain only $\sim 3,000$ stars, appropriate for open clusters, we have started to use the next-generation special-purpose computer, the GRAPE-6, to extend our simulations to include one or two orders of magnitude more stars. This will enable us to model globular clusters on a star-by-star basis, including those with very dense cores where most stars are influenced by various ‘traffic accidents’ in the form of encounters and mergers. The simulations reported here thus play a double role: astrophysically, they provide insight in the evolution of open clusters, and computationally, they help pave the way for the modeling of the more complex globular clusters.

In this paper we describe a series of self-consistent simulations of the evolution of open star clusters. All important effects are included to some degree of realism: stellar evolution, binary evolution, the internal dynamical evolution and the effects of the tidal field of the Galaxy. This is the fifth paper in a series in which we have gradually increased the ‘ecological’ complexity of stellar interactions to a realistic level. In this paper we analyze the results of the same eight calculations performed for our previous Paper IV (Portegies Zwart et al. 1999). There we concentrated on global

cluster properties and compared them with observed open clusters, such as the Pleiades, Praesepe and Hyades. Specifically, we took a photometric standpoint and studied changes in the Hertzsprung-Russell diagram and cluster morphology as functions of time and initial conditions. Here we concentrate on the binary population and on higher-order multiple systems, and we study the dynamical and observational effects of these binaries and multiples on the evolution of the stellar system as a whole.

Detailed descriptions of the numerical methods used and global assumptions made in our calculations are given in Paper IV. Since we analyze the same data from a different perspective we do not repeat this information here. Instead, we quickly review the initial conditions of our models, and restate the methods used; for more details, see Paper IV.

2 METHODS

In this section we briefly discuss the initial conditions of our models and the numerical techniques used in our model calculations. For details, refer to Appendix B and C of Paper IV (Portegies Zwart et al. 1999).

Table 3. Initial conditions for the stellar and binary population. The first column gives the parameter, the second column gives the functional dependence, followed by the lower and upper limits adopted. (RLOF indicates that the initial binary may be semi-detached.)

parameter	function	lower	upper
mass function	Scalo	0.1 M_{\odot}	100 M_{\odot}
secondary mass	$P(m) = \text{constant}$	0.1 M_{\odot}	$M_{\text{prim}}/M_{\odot}$
orbital separation	$P(a) = 1/a$	RLOF	5000 AU
eccentricity	$P(e) = 2e$	0	1

2.1 Initial conditions

We are interested in moderately rich (~ 1000 stars) open clusters of intermediate age ($\lesssim 1$ Gyr). Starting from the currently observed mass and dynamical properties of such clusters we have reconstructed two plausible sets of initial conditions, which are presented in Table 2. Each calculation is performed four times with different random seeds in order to improve statistics. The notation in this paper is identical to that used in Paper IV (see its Appendix A for an overview).

For our simulations we assume a Scalo (1986) initial mass function, with minimum and maximum masses of 0.1 M_{\odot} and 100 M_{\odot} , respectively, and mean mass $\langle m \rangle \simeq 0.6 M_{\odot}$ at birth. Consistent with the above mass estimates, our simulations are performed with 1024 single stars and 1024 binaries, for a total of 3096 (3k) stars.

Stars and binaries within our model are initialized as follows. A total of 2k single stars are selected from the initial mass function and placed in an equilibrium configuration in the selected density distribution (see below). We then randomly select 1k stars and add a second companion star to them. The masses of the companions are selected randomly from the IMF between 0.1 M_{\odot} and the primary mass (see Tab. 3). For the adopted binary fraction, the restricted secondary mass range translates into an overall mean mass of 0.53 M_{\odot} . Then the other binary parameters are determined. Binary eccentricities are selected from a thermal distribution between 0 and 1. Orbital separations a are selected with uniform probability in $\log a$ between Roche-lobe contact and an upper limit of 5,000 A.U. ($= 10^6 R_{\odot}$, or 0.02 pc). When a binary appears to be in contact at pericenter, that particular orbit choice is rejected and new orbital parameters are selected. Table 3 gives an overview of the various distribution functions from which stars and binaries are initialized. (Figure 4 shows the initial distributions of orbital period and eccentricity.)

We select initial density profiles from the density distributions described by Heggie & Ramamani (1995) with $W_0 = 4$ and $W_0 = 6$, and refer to these models as W4 and W6, respectively, throughout this paper. We have performed four independent simulations for each set of initial conditions, labeled I to IV.

All our cluster models start with the same virial radius of $R_0 = 2.5$ pc. This implies a conveniently constant scaling between the cluster dynamical time scale $\sim (GM_0/R_0^3)^{-1/2}$ ($= 1.5$ Myr for $M_0 = 1600 M_{\odot}$) and the time scale for stellar evolution. Each cluster is assumed to precisely fill its Jacobi surface at birth. Given the observed Oort constants in the

solar neighborhood, we find that a model with $W_0 = 6$ has to be placed slightly farther (10.4 kpc) from the Galactic center than the Sun, while a model with $W_0 = 4$ has to reside somewhat closer (6.8 kpc), in order to obey the above relationships.

For a total cluster mass of 1600 M_{\odot} , the Lagrange points of our two standard clusters lie at distances 14.5 pc ($W_0 = 4$) and 21.6 pc ($W_0 = 6$), from the cluster center. Stars are removed from a simulation when their distance to the cluster's density center exceeds twice the distance to the first Lagrangian point. Table 2 reviews the selected parameters and initial conditions.

2.2 The N -body integrator

The N -body integration in our simulations is carried out using the kira integrator, operating within the Starlab software environment (McMillan & Hut 1996; Portegies Zwart et al. 1999). Kira uses a fourth-order Hermite scheme (Makino & Aarseth 1992), incorporates block time steps (McMillan 1986a; 1986b; Makino 1991), includes special treatments of close two-body and multiple encounters of arbitrary complexity, and a robust treatment of stellar and binary evolution and stellar collisions (see below). As mentioned above, the special-purpose GRAPE-4 (Makino et al. 1997) system is used to accelerate the computation of gravitational forces between stars.

2.3 Stellar evolution

The evolution of the stars is adapted from the prescription by Portegies Zwart & Verbunt (1996, §2.1). However, some changes are made to the mass loss in the main-sequence stage for massive stars and for mass-transfer remnants. We follow the details of model B from Portegies Zwart & Yungelson (1998). For our treatment of stellar mass loss, see Portegies Zwart et al. (1998).

Neutron stars receive a high-velocity kick at the moment of their formation. The reasons for the occurrence of these high kick velocities have been discussed in detail by Portegies Zwart & van den Heuvel (1999) and the implications for binary evolution are discussed by Portegies Zwart (2000). The distribution from which the kick velocity should be taken is less certain. We adopt the velocity distribution proposed by Harmann (1997) which has a dispersion velocity of 450 km s^{-1} . Each neutron star formed received a kick chosen from this distribution and oriented in a random direction.

3 RESULTS

3.1 Overall evolution of the models

In this section we review the global properties of models W4 and W6, summarizing the more extensive discussion presented in Paper IV. Where we discuss individual models, we focus on the same two models discussed in Paper IV (model W4-IV and W6-III). In other cases the data for several models, or even all models, are combined in order to improve statistics; those cases are indicated specifically below.

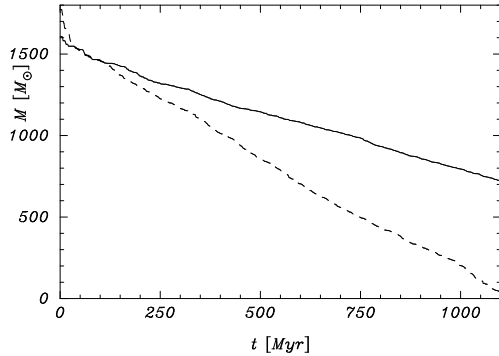


Figure 1. Total mass as a function of time for model W4 (dashes) and W6 (solid).

Figures 1 and 2 present the overall evolution for our two sets of cluster initial conditions. Figure 1 shows the time evolution of the cluster mass. Models W4 and W6 lose mass at roughly constant rates of about $1.4 M_{\odot}$ (0.09%) and $0.82 M_{\odot}$ (0.05%) per million years, respectively. These mass loss rates result in the disruption of the cluster at about 1 Gyr for model W4 and around 2 Gyr for the more concentrated model W6. The higher mass loss rate of model W4 is mainly attributable to its closer proximity to the Galactic center and not per se to its lower concentration. These rates are consistent with a mass loss rate of $1.2 M_{\odot}$ per million years for the slightly more massive star cluster studied by Hurley et al. (2001; 2002). The mass-loss rates per half mass relaxation time derived by Portegies Zwart et al. (2001) for dense star clusters near the Galactic center are about a factor of four higher than the corresponding rates for the clusters studied here.

Figure 2 shows the evolution of the Lagrangian radii containing 5%, 25%, 50% and 75% of the cluster mass, for models W4 and W6. Both clusters expand by about a factor of three during the first half-mass relaxation time (~ 140 Myr). It is not clear whether the clusters experience any significant core collapse during this early phase. In Paper IV we concluded that the clusters do not experience core collapse due to the effects of binary activity, which tends to counteract core contraction (see McMillan et al. 1990, 1991). At later times ($t \gtrsim 650$ Myr for model W4 and somewhat later for model W6), the Lagrangian radii decrease again as the cluster starts to dissolve in the tidal field of the Galaxy.

3.2 Global binary properties

Both models start with 50% binaries, so two-thirds of the stars are initially members of binary systems. The adopted upper limit ($10^6 R_{\odot}$) on the initial semi-major axis means that most initial binaries are relatively wide. The fraction of hard ($|E| \gtrsim 1kT$) binaries was 0.46 ± 0.01 for all models, irrespective of the initial density profile. (The thermodynamic unit kT is defined in Paper IV).

Figure 3 shows the evolution of the binary fraction. Shortly after the start of the runs, the binary fractions drop to about 42% and 48% for models W4 and W6, respectively, and remain roughly constant thereafter. This initial decrease

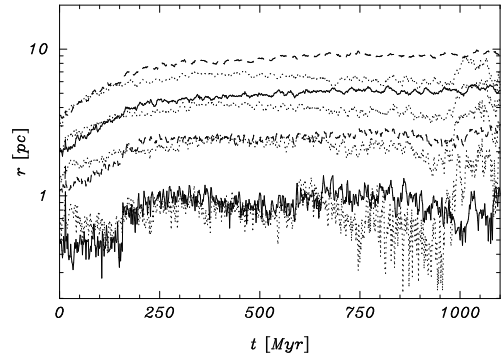


Figure 2. Evolution of the 5%, 25%, 50% and 75% Lagrangian radii for model W6 (solid lines for the 5% and 50%, dashed lines for the 25% and 75% Lagrangian radii). Lagrangian radii for model W4 are presented as dotted lines.

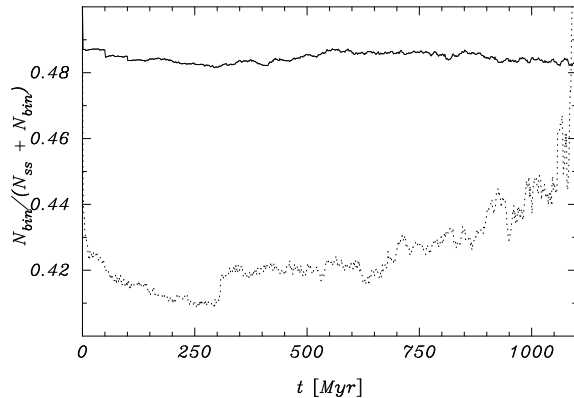


Figure 3. Binary fractions as a function of time for models W4 (dotted line) and W6 (solid line).

in binary frequency is consistent with the disruption of all soft ($|E| \lesssim 1kT$) binaries. Supernova explosions dissociated 1.8% of the binaries in the W4 models, and about half that number in the W6 models. This difference is mainly the result of random fluctuations. Fluctuations in the binary fraction after ~ 100 Myr are mainly the result of escapers and mergers. The number of mergers resulting from unstable mass transfer or direct collisions is $12.1 \pm 0.5\%$ for models W4 and W6. The escape rate of binaries closely follows the escape rate of single stars; both are relatively constant with time. Model W6 loses one binary per 2Myr; the escape rate for model W4 is about twice as high.

3.3 Evolution of binary parameters

The ecological interplay between stellar (and binary) evolution, stellar (and binary) dynamics, and the external tidal influence of the Galaxy transforms the initial distributions of stars and binaries in complex ways. We assume that initially all binaries are distributed throughout the cluster in the same way as single stars. However, since binaries are on average more massive than single stars, they subsequently tend to sink to the cluster center, where superelastic encoun-

ters quickly modify the spatial distributions of both stars and binaries.

These encounters come in many forms, from the more common single-star–binary and binary–binary types to the rare forms that involve triples and occasionally even higher-order multiple systems. The combined effects of such encounters significantly modifies the binary distribution functions, in terms of radius and binding energy as well as stellar type. In addition, stellar evolution and isolated binary evolution also cause binary parameters to evolve in time, independent of the occurrence of dynamical close encounters. In this subsection, we will present some of the net results of these complex processes.

3.3.1 Distributions of orbital period and eccentricity

Figure 4a shows the initial distribution of orbital period (in years) and eccentricity of a subset of the primordial binaries of model W6 (the initial conditions for model W4 are identical). Figures 4b and c show the same distributions for models W4 (panel b) and W6 (panel c) at 600 Myr. In the middle panel, for model W4, only 871 binaries remained. In order to facilitate visual comparison, the upper and lower panels also show only 871 binaries out of the larger numbers that could have been plotted.

A striking feature of the three panels in Fig 4, is the lack of wide ($p_{\text{orb}} \gtrsim 10^4$ yr) binaries at later times. These binaries are completely absent in model W4, while in model W6 a small population of wide binaries remains. This deficiency in wide binaries in evolved clusters is caused by ionization of the soft binaries by dynamical encounters (see also Figure 3). For model W4 this process is more efficient than for the more concentrated models because 1) the W4 models experience a high density phase during their early evolution, and 2) the W6 models have extended outer regions with relatively low stellar densities because of the weaker tidal field. All surviving binaries with $p_{\text{orb}} \gtrsim 10^5$ year are located well beyond the cluster's half mass radius, and most contain at least one white dwarf. In many cases, the orbital periods of these non-interacting binaries has increased substantially due to the large amount of mass lost from one (or both) of the component stars.

Binaries located above and to the left of the left-most dotted curves experience strong tidal effects during their early evolution. As a result, they quickly circularize, as can be seen by their precipitation to the zero-eccentricity line at the bottom in the last two panels. The majority of these systems contain at least one white dwarf or helium star. Occasionally a binary may enter the 'forbidden' left-most area at a later time as a result of a strong dynamical encounter. Such a binary will either be quickly circularized or its components will collide and merge to form a single star (see §3.5).

Figure 5 shows how the percentage of tidally circularized binaries evolves over time. Not surprisingly, the very hard binaries, which have high binding energy and therefore tight orbits, have on average undergone much stronger tidal interactions and therefore have had a much larger chance to circularize. The four percentages presented in the figure—hard binaries and all binaries for each of the two classes of model—at first change little during the evolution of the

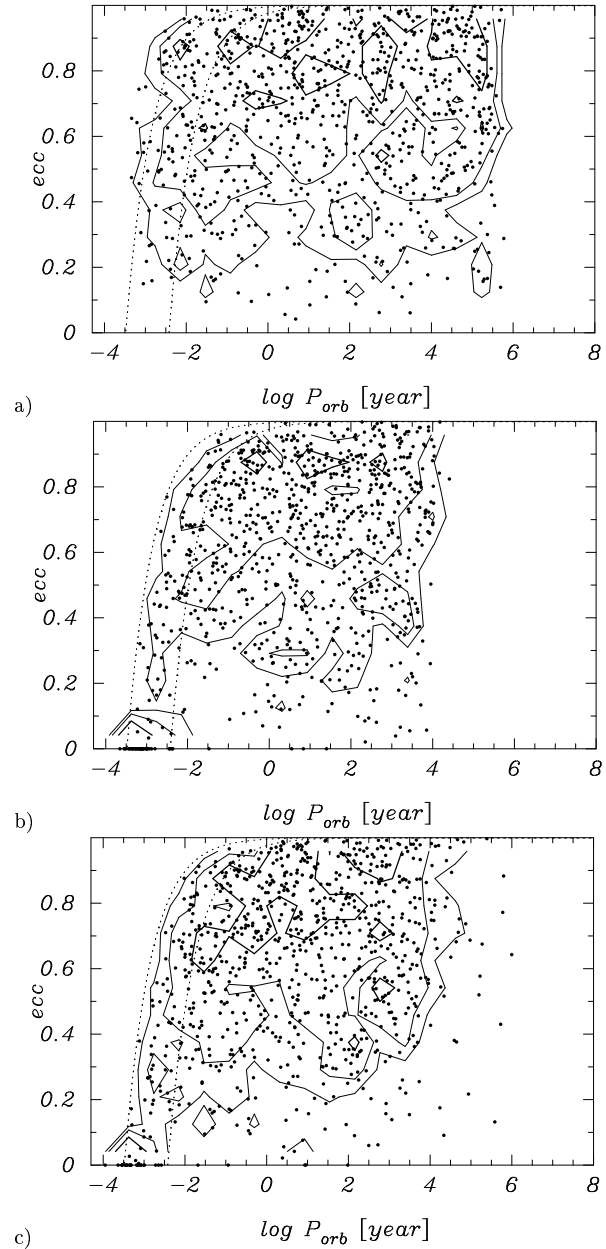


Figure 4. Scatter plots for the orbital period versus the eccentricity for 871 binaries for various models and moments in time: a) initial distribution, b) the distribution for model W4 at an age of 600 Myr, c) model W6 at $t = 600$ Myr. Each panel is constructed using 871 binaries. Contours give the 0.5, 0.25 and 0.125 iso-density curves of the distribution in the two coordinates plotted here. The left dotted curve indicates at which orbital period and eccentricity a binary with a $0.1 M_{\odot}$ zero-age primary circularizes during the time span of our simulations. The right dotted curve is for a $2.26 M_{\odot}$ primary at zero age.

cluster, but they increase at later times in the case of model W4.

Note that in Fig 4 there are some circularized binaries with long orbital periods, far to the left of the right-most dotted line, in the middle and lower panel. These are absent in the upper panel, which shows the initial conditions. The tidal circularization of these systems occurred when one of the stars ascended the giant branch before the onset of mass

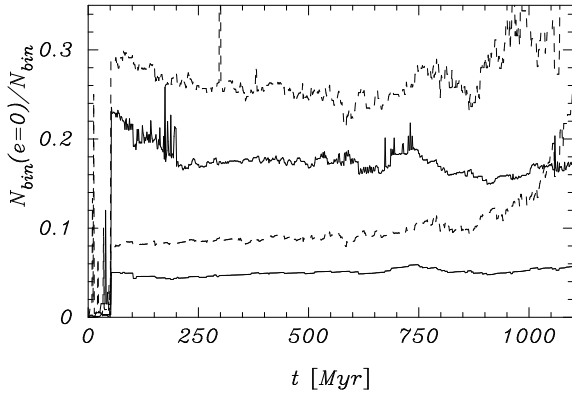


Figure 5. The relative number of binaries that are tidally circularized, as a function of time, for the models W4 (dashed lines) and W6 (solid lines). In each case, the lower lines present the overall fraction of binaries that are circularized, while the top curves indicate the fraction of circularized binaries among those binaries that are very hard ($|E_{\text{bin}}| \gtrsim 1000kT$).

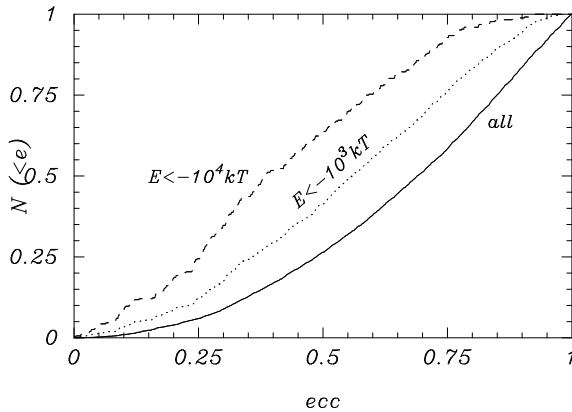


Figure 6. Cumulative distribution of the binary eccentricity. Solid line, initial conditions (the thermal distribution). The dashed and dotted line represent the eccentricity distributions at an age of 600 Myr of binaries with a binding energy $E_{\text{bin}} < -10^3kT$ and $E_{\text{bin}} < -10^4kT$, respectively. For the latter two curves the data for all models W4 and W6 are combined. However, we excluded those binaries which have been circularized by tidal forces.

transfer. While in many cases this type of evolution leads to a later shrinking of the orbit, in some rare cases the binaries remain wide after a period of modest mass transfer.

Since tidal forces drop off quickly with distance, in most cases they either succeed in fully circularizing a binary, or they do not cause much of an effect. Consequently, the eccentricity distribution of most non-circularized binaries changes little with time. Figure 6 illustrates this by presenting the cumulative distribution of all binaries with the exception of those with zero eccentricity. Note that this general argument does not hold for the hardest binaries: when we select only the hard ($|E_{\text{bin}}| \gtrsim 1000kT$) or super-hard ($|E_{\text{bin}}| \gtrsim 10^4kT$) binaries, clear deviations from the initial thermal distribution are evident. This is not surprising: a 10^4kT binary simply does not have enough room to develop an eccentricity of, say, 0.9, because the semimajor axis is too small.

3.3.2 Radial distribution of binaries

Figure 7 shows the binary fraction as function of distance to the cluster center at birth and at $t = 600$ Myr, adopted as a representative snapshot of an older cluster. (Qualitatively similar results would have been obtained had we selected any other time between ~ 200 Myr and 1 Gyr.) The upper solid line shows the initial distribution for all binaries, regardless of their binding energy. The lower solid line presents the initial fraction of binaries with a binding energy of at least $|E_{\text{bin}}| > 1000kT$. To avoid clutter, we have shown the statistical uncertainties in the form of error bars only for the bullet points; the uncertainties in the open and close triangles can be estimated by the scatter between neighboring points.

The triangles in Figure 7 shows the distribution for all binaries at $t = 600$ Myr for model W6 (open) and for model W4 (filled). The two distributions show similar trends, except for a generally smaller binary fraction in model W4 (see also Figure 5). The binary fraction in the central portion of the cluster is considerably higher than it was initially (upper solid line), because of mass segregation. For higher r values, the fraction of objects that are binary remains below the original value, all the way to and beyond the tidal radius.

The bullets indicate the distribution of binaries with $|E_{\text{bin}}| > 1000kT$ at a cluster age of 600 Myr. In order to improve our statistics, we have combined the data from the two models; the distributions are similar, with model W6 containing $\sim 8\%$ more hard binaries than model W4. Note that we find a higher proportion of hard binaries over the entire cluster field as compared to the initial distribution. This is mainly a result of dynamical evolution: hard binaries tend to get harder, and therefore some of the binaries contributing to the bullet points started off with a binding energy less than $1000kT$, and thus were not counted in the construction of the lower solid line.

The higher central concentration of very hard binaries, as compared to less hard binaries, is evident in Figure 8, which figure shows the cumulative distribution for single stars, hard $|E_{\text{bin}}| > 1000kT$ and super hard $|E_{\text{bin}}| > 10^5kT$ binaries. The figure also presents the cumulative radial distribution for higher order (mostly triple) systems. The left-most and right-most dotted curves in Figure 8 show the radial distribution for model W6 at birth and at an age of 600 Myr, respectively. Initially, both single stars and binaries follow the left-most dotted curve. At an age of 600 Myr, all binaries are more centrally concentrated than the single stars (see the figure caption). The harder the binaries, the more centrally concentrated their distribution has become. In the case of triples, the condensation toward the center is extreme, with a triple half-mass radius of around 0.3 pc.

The high central concentration of the very hard $|E_{\text{bin}}| > 10^5kT$ binaries is in part due to their early history. These binaries are largely the product of an unstable phase of mass transfer. The stellar components in these binaries were therefore more massive than they are at $t = 600$ Myr, so they are more strongly affected by mass segregation, causing them to sink to the central regions. In contrast, the moderately hard binaries with binding energies between $100kT$ and $10kT$ (not shown in Figure 8) are barely more centrally concentrated than the single stars. The triples are strongly centrally concentrated. This is a the most dramatic result

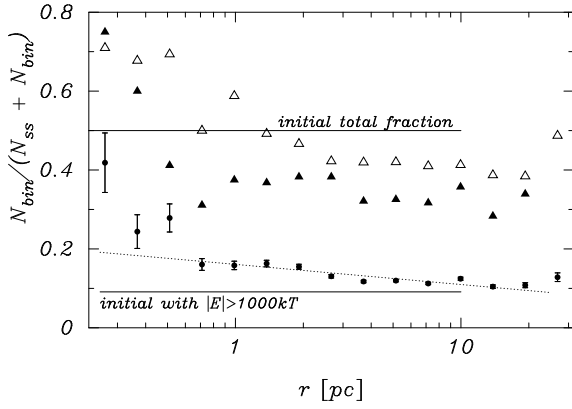


Figure 7. Fraction of binaries $N_{\text{bin}}/(N_{\text{ss}} + N_{\text{bin}})$ as function of the distance to the cluster center. The upper solid horizontal line shows the initial binary fraction over the entire star cluster. The cut off at about 10 pc is close to the location of the tidal radius. (Initially there were no stars beyond the tidal radius.) The lower solid curve presents the initial distribution for binaries with $|E_{\text{bin}}| > 1000kT$. The open triangles give the distribution of all binaries for model W6 at an age of 600 Myr. The solid triangles present the distribution of all binaries for model W4 at an age of 600 Myr. The bullets (with 1σ Poissonian error bars) present the fraction of hard $|E_{\text{bin}}| > 1000kT$ binaries as a function of the distance to the cluster center at an age of 600 Myr. These data combine models W4 and W6. To guide the eye we have placed a straight (dotted) line through these bullet points.

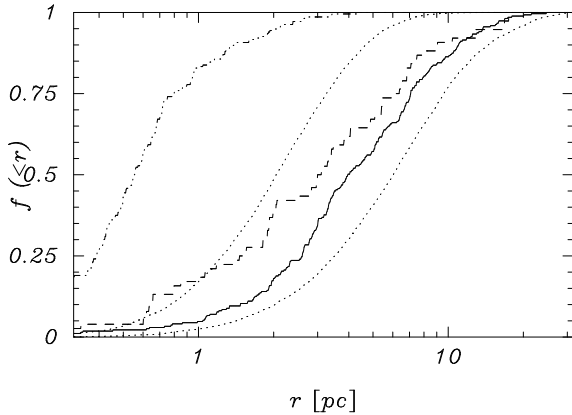


Figure 8. Cumulative radial distribution of single stars and binaries in models W4 and W6 (combined). The cumulative distribution for all single stars and binaries at birth and at $t = 600$ Myr are given by the left and right dotted curves, respectively. The solid curve gives the distribution for binaries with $|E_{\text{bin}}| > 10^3kT$ at an age of 600 Myr. The dashed curve gives the same distribution for $|E_{\text{bin}}| > 10^5kT$ binaries. The dash-3-dotted curve gives the radial distribution for higher order (mostly triple) systems. To improve statistics we accumulated all triples for models W4 and W6 over the time range of 550 Myr to 650 Myr.

of dynamical interactions: triple systems were not initially present, and must be created dynamically through encounters. Since the encounter rate increases sharply toward the cluster center, triples and higher-order systems are born, and often quickly destroyed again, near the very center of the cluster.

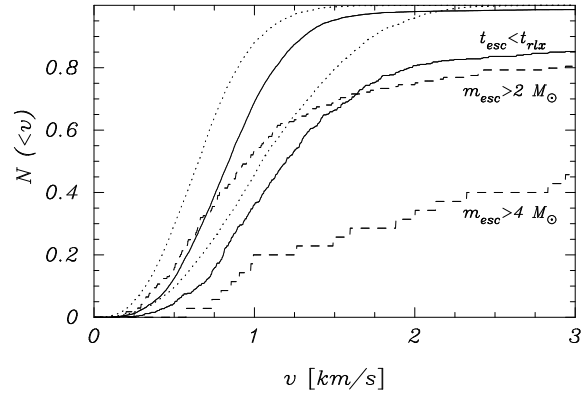


Figure 9. Cumulative distribution of the velocities of escaping single stars and binaries in models W4 and model W6 (combined). The two dotted lines show the velocity distributions of single stars in the models at zero age (right) and at $t = 600$ Myr (left). The left solid curve presents the distribution of the escaper velocity of all stars and binaries integrated over time. The right solid curve gives the velocity distribution of stars which escaped within the first half-mass relaxation time (~ 150 Myr). The two dashed curves give the escape speeds for stars with masses $m_{\text{esc}} > 2 M_{\odot}$ (upper) and $m_{\text{esc}} > 4 M_{\odot}$ (lower).

3.4 Escapers

The most important mechanism by which stars escape from the cluster is tidal stripping. Stars are assumed to have been tidally stripped once they reach two Jacobi (tidal) radii from the cluster center; they are then removed from the simulation. Stripped stars generally leave the cluster with relatively low velocities, as illustrated in Figure 9, which shows the distribution of escaper speeds for models W4 and W6.

It is convenient to draw a distinction between tidal evaporation and dynamical ejection of stars. Operationally, we distinguish between the two processes by the speed of the escaper; an “ejected” single star or binary leaves the cluster with a speed exceeding the escape velocity. That is, we infer the dynamics from the speed. Typically, this velocity is imparted to the escaping object during a strong interaction with another object in the cluster core. Because of the relatively low central densities (and hence low reaction rates) in our model clusters, this type of ejection is rather uncommon. White dwarf ejection velocities are not significantly different from those of main sequence stars, but giants have on average somewhat lower escaper velocities. This is mainly a consequence of the fact that giants are generally large and therefore cannot have very close encounters without colliding, so they are less able to pick up large escape velocities.

Another important escape mechanism is supernova explosions. A neutron star formed in a core-collapse supernova is hurled into space with a “kick” velocity that can easily exceed several hundreds of kilometers per second, greater than the cluster escape speed by 1–2 order of magnitude. These objects are hidden in the high-velocity tail of Figure 9; however, they are clearly visible in Figure 10 as the population of high-speed single objects with masses between $1 M_{\odot}$ and $2 M_{\odot}$.

A supernova in a binary system has several effects on the velocity distribution of both single and binary stars. The sudden mass loss in the supernova event, as well as

the asymmetric velocity kick, affect a binary's internal orbital parameters and its center of mass velocity. When the binary is dissociated in the supernova, the companion to the exploding star is ejected with its orbital velocity, while the newly formed compact object receives an additional velocity kick. The effects of supernovæ on binary systems, and on the velocities of the binaries and single stars which result, are reviewed by Portegies Zwart (2000).

Figure 9 shows the velocity distribution of escaping stars and binaries from models W4 and W6. Due to the similarities in escape speeds between the two models, we have combined the data in a single plot. The escaper velocity distribution for single stars is slightly higher than that of the binaries. For clarity we show only the combined distribution of single and binary escapers in Figure 9. Escaper velocities are generally only slightly higher than the cluster velocity dispersion, and somewhat higher in the W4 models than in W6. The small fraction of high-velocity escapers in Figure 9 is due to neutron stars escaping after supernovae explosions.

In addition to the overall escaper velocities for the combined models, Figure 9 also shows the distribution for stars which escaped within the first half-mass relaxation time (right solid line). This distribution has a considerably higher mean than the overall distribution. The figure also shows the velocity distributions for escaping stars more massive than $2 M_{\odot}$ (top dashed curve) and $m_{\text{esc}} > 4 M_{\odot}$ (lower dashed). These distributions are very different from the average escaper speed. Both models W4 and W6 experience high-density phases during their early evolution, within 1 initial half-mass relaxation time. The early escapers therefore have higher velocities. A similar process operates for the more massive escapers. The turn-off mass of a $2 M_{\odot}$ star is about 800 Myr, while a $4 M_{\odot}$ star lives for less than about 140 Myr. The distribution of escaper speeds for stars which escaped within t_{rlx} includes the stars with $m > 4 M_{\odot}$. Still, the distributions are considerably different, in the sense that the massive stars have relatively high escape speeds. The reason for this discrepancy is the greater dynamical activity of the high-mass stars, which take part much more often in dynamical encounters with binaries.

The dependence of escaper velocity on escaper mass is illustrated in Figure 10. Most escapers have low masses and low velocities. The average escaper velocity in the W4 and W6 runs was 1.14 km s^{-1} and 1.00 km s^{-1} , respectively. Higher mass stars (and binaries) have considerably higher velocities. This trend was first observed by Blaauw (1961, see also Gies & Bolton 1986). Binaries are mostly ejected by dynamical encounters. Supernovae are also responsible for numerous high velocity escapers, both from kicks and from binary effects, as mentioned above. The neutron stars are clearly visible in Figure 10 as the objects having masses of about $1.4 M_{\odot}$ and velocities up to $\sim 1000 \text{ km s}^{-1}$.

Two rather low-mass ($m \sim 0.11 M_{\odot}$ and $m \sim 0.7 M_{\odot}$) stars have unusually large ($\sim 100 \text{ km s}^{-1}$ and 185 km s^{-1} , respectively) escape velocities. The more massive of the two was ejected from a tight binary at about $t = 5.6 \text{ Myr}$ when its companion exploded in a Type Ib supernova, dissociating the binary. The low-mass object was ejected following a three-body encounter at $t = 223 \text{ Myr}$.

Of all stars ejected from models W4 and W6, only 109 ($\sim 0.93\%$ out of a total of roughly 12,000) have velocities

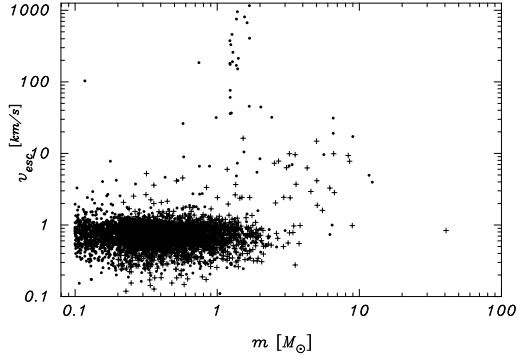


Figure 10. Mass versus velocity for escaping single stars (dots) and binaries (plus signs) in model W6. For the binaries, the total mass is used.

exceeding three times the dispersion velocity v_{disp} of the parent cluster. Of these, 46 are neutron stars. However, 57% of escapers with masses between $4 M_{\odot}$ and $11 M_{\odot}$, and 75% of escapers more massive than $11 M_{\odot}$, have velocities more than $3v_{\text{disp}}$. The average escaper velocity of stars between $4 M_{\odot}$ and $11 M_{\odot}$ is 8.5 km s^{-1} ; stars with masses exceeding $11 M_{\odot}$ have an average escaper velocity of 21 km s^{-1} , which is much higher than the cluster dispersion velocity.

These numbers are unusually high compared to the number of runaways in the Galactic disk. However, as our criterion here we have adopted three times the cluster velocity dispersion, instead of Blaauw's (1961) criterion of 40 km s^{-1} (or three times the velocity dispersion in the Galactic disk). The fraction of high velocity stars following Blaauw (1961) was between $\sim 1\%$ for stars with $m \lesssim 11 M_{\odot}$, about 2.5% for early B stars and about 20% among O stars ($m \gtrsim 16 M_{\odot}$, see also Sone 1991). Among stars of spectral type A, Stone (1991) found a runaway frequency of $\lesssim 0.3\%$. These numbers are consistent with binary population synthesis studies of binaries in which stellar dynamical encounters are not taken into account (Portegies Zwart 2001).

The velocity dispersion of all stars in the cluster at an age of 600 Myr is $v_{\text{disp}} = 0.72 \pm 0.23 \text{ km s}^{-1}$. For stars within 1 pc (about the core radius) of the cluster center, $v_{\text{disp}} = 0.98 \pm 0.34 \text{ km s}^{-1}$; stars between 10 and 15 pc of the center have $v_{\text{disp}} = 0.59 \pm 0.16 \text{ km s}^{-1}$. Most striking is the higher velocity dispersion for stars well outside the tidal radius ($r > 15 \text{ pc}$) which have $v_{\text{disp}} = 0.75 \pm 0.20 \text{ km s}^{-1}$. A KS test indicates that the various velocity distributions are significantly different.

Drukier et al. (1998) reported a similar effect in the Globular cluster M15, and attributed it to tidal shocking. However, this process is not included in our models; we therefore conclude that the observed increase in the velocity dispersion outside the tidal radius cannot simply be a consequence of tidal shocks.

3.5 Collisions and Coalescence

Stellar mergers result from unstable mass transfer in a binary system or from direct collisions between stars. Some-

Table 4. Mergers occurring in models W4 and W6, compared with those in model calculations published previously. The first column identifies the two stars involved in the merger. The next two columns give the number of mergers in each model calculation, followed by the fraction of each merger type (expressed as a percentage, combining all runs). The last two columns give the fractions of mergers which occurred in models S of Papers I and II. Mergers between two remnants in Paper II (model S) are included here under {wd, wd}, although a few actually involved a neutron star or black hole.

Ntot:	W4	W6	total	Paper IS [%]	Paper IIS
{ms, ms}	92	110	84	77	80
{ms, gs}	19	11	12	14	6
{ms, wd}	0	1	0	5	11
{ms, ns}	1	0	0	1	1
{gs, ns}	0	0	0	3	0
{wd, wd}	5	0	2	0	2
{wd, ns}	0	2	1	0	0

times (unstable) mass transfer is initiated by the presence of a third star.

Table 4 gives an overview of the 241 collisions occurring during the model calculations discussed here. A schematic diagram of the relative frequencies of various collision configurations is presented in Figure 11. This figure may be compared directly with Figure 2 of Paper I, and with Figure 5 of Paper II. For easier comparison, we have added to Table 4 two columns summarizing the results of Papers I and II. Note, however, that the comparison with papers I and II is not really appropriate, as these model calculations lasted for 10 Gyr. According to a KS test there is no significant difference between the time histories of the collisions in the W4 and the W6 models.

Most ($\gtrsim 80\%$) mergers in models W4 and W6 occur between two main sequence stars (see Table 4). This was also the case in Papers I and II. In Paper I, however, only collisions between single stars were considered, and the high proportion of main-sequence collisions simply reflects the high proportion of main-sequence stars. Paper II included both collisions between single stars and mergers resulting from binary mass transfer, so the results in that case should compare better with models W4 and W6. The collisions reported in this paper, however, have a rather small contribution from {ms, wd} mergers compared to those in Papers I and II. This may be due in part to the smaller ages ($\lesssim 1$ Gyr) of our models compared with Papers I and II (< 10 Gyr).

Although clearly limited by small number statistics, an apparent difference between models W4 and W6 is the number of {wd, wd} mergers, which are much more common in model W4. This difference is reflected in the higher Type Ia supernova rate in model W4. Interestingly, the calculations in Paper II also had a high {wd, wd} merger fraction. In fact, if the binary population of models W4 and W6 were allowed to evolve after the disruption of the cluster, the rate of {wd, wd} mergers would be very similar to the results of Paper II. The cause of the high proportion of white-dwarf mergers in model W4 and Paper II is the larger amount of dynamical activity in these models, which drives more binaries into a state of mass transfer, favoring the formation

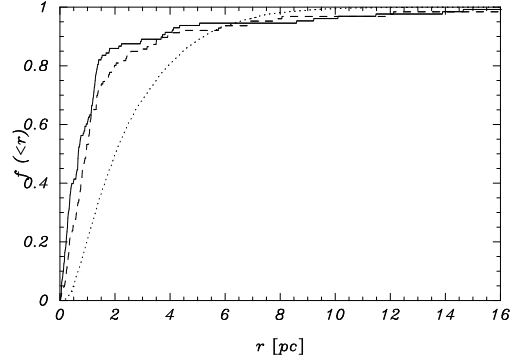


Figure 12. Cumulative distribution of the distance from the cluster center at which collisions occur in models W4 (dashes) and W6 (solid). The dotted line gives the initial distribution of stars in the W6 models.

of white-dwarf binaries (see also Hurley & Shara 2002). The resulting Type Ia supernova rate is discussed in the next section.

Figure 12 shows the radial distribution of collisions in models W4 and W6. More than 80% of all collisions occur within the initial half-mass radius (~ 3 pc). Collisions in the W6 models tend to be more concentrated to the cluster core than in the W4 models. It is striking that some ($\sim 5\%$) collisions occur far ($\gtrsim 8$ pc) from the cluster center. These collisions are induced by binary evolution, whereas mergers in the core are mainly caused by stellar encounters.

The expected distribution of masses and radii of colliding stars can be calculated following Portegies Zwart et al. (1997; see their Eq. 14). Assuming a Maxwellian velocity distribution with velocity dispersion v and including the effects of gravitational focusing, the number of collisions in the cluster per 10^8 year may be expressed as

$$\Gamma \approx \left(\frac{n}{10^3 \text{ pc}^{-3}} \right)^2 \left(\frac{r_{\text{core}}}{\text{pc}} \right)^3 \left(\frac{m}{M_{\odot}} \right) \left(\frac{d}{R_{\odot}} \right) \left(\frac{\text{km s}^{-1}}{v} \right), \quad (1)$$

where m is the stellar mass. This rate is averaged over all other masses. (Note that, based on this estimate, we expect no collisions during the time span of our simulations for our adopted cluster parameters, underscoring the importance of binary interactions.)

Figure 13 shows the expected (upper panel; see paper III for details) and observed (lower panel) distributions of primary and secondary masses of stars involved in collisions in models W4 and W6. We excluded here the stars which merged as a result of unstable mass transfer. The upper panel is created via Eq. 1 from the initial mass function and the same mass-radius relation for zero-age main-sequence stars as was used in the model calculations. Gray shades indicate collision probability; darker shades correspond to higher values. The collisions observed in our models are presented in the lower panel. The masses of the colliding components in our model calculations are on average somewhat higher than expected. This phenomenon was first observed by Portegies Zwart et al. (1999; see also Portegies Zwart & McMillan 2002) in simulations of young star clusters having high central stellar densities. Portegies Zwart et al (1999)

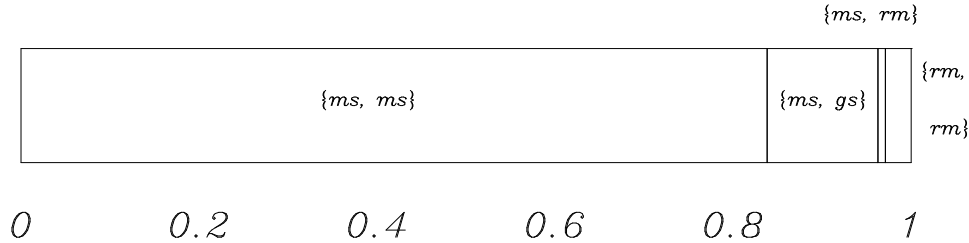


Figure 11. Schematic overview of the relative frequencies of mergers between various stellar types in models W4 and W6 (combined). Stellar types are denoted by *ms* for main sequence, *gs* for (sub)giants and *rm* for white dwarfs and neutron stars. Table 4 gives the numbers of occurrences.

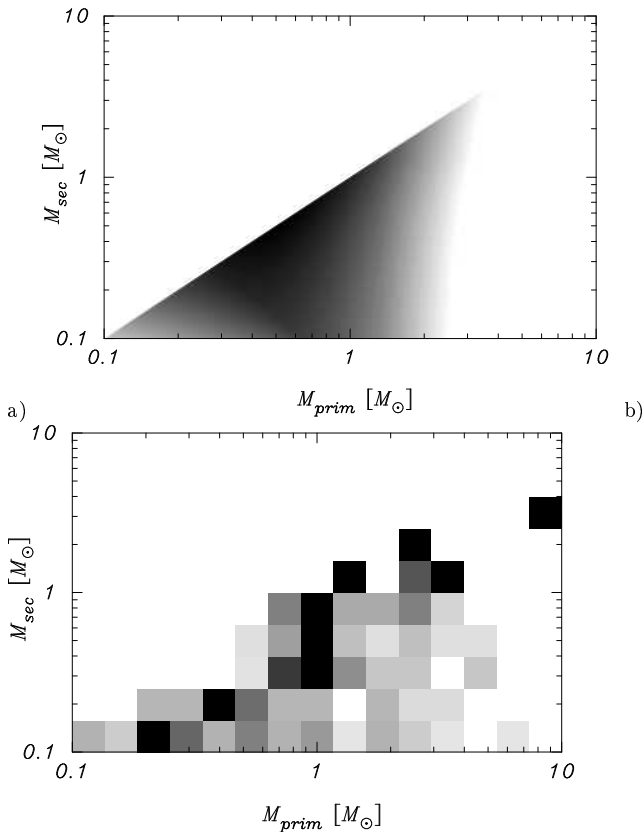


Figure 13. Relative collision rates between a primary and a secondary star as expected from Eq. 1 (upper panel), and as found in models W4 and W6 (lower panel). For the lower panel the mergers which resulted from an unstable phase of mass transfer are excluded; only the true collisions are taken into account. The shading is linear in the encounter probability in the upper panel and in the number of collisions in the lower panel. Darker shades indicate higher collision frequency. Since the probability distribution is symmetric about the line of equal masses, only the lower half of each figure is displayed.

used R136, a compact and very dense star cluster in the 30 Doradus region, as template for their simulations. We return to this comparison in the discussion section.

For 240 of the 241 stellar pairs experiencing a collision, we were able to reconstruct the orbit before the collision occurred. Figure 14 shows the orbital parameters for the bound

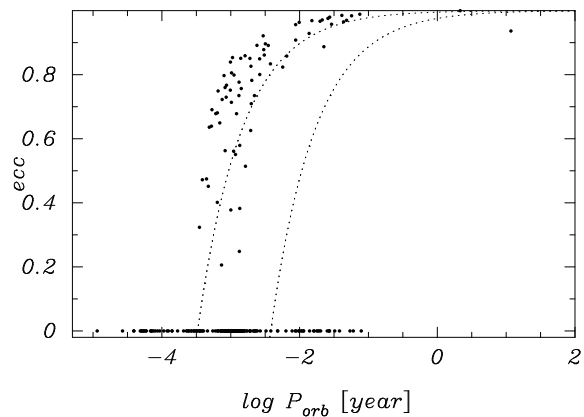


Figure 14. Orbital periods and eccentricities of coalescing binaries in models W4 and W6. Notice the rather large population of circular (zero eccentricity) binaries which experience a collision.

systems thus obtained. The single pair for which this reconstruction was not possible experienced a collision during a supernova event—the neutron star formed in the supernova was ejected directly into its $1.9 M_{\odot}$ main-sequence companion. In 181 of the 240 collisions ($\sim 71\%$), the orbit was circular on merger. The eccentricity distribution in the other bound cases is consistent with a thermal distribution. This result is consistent with the findings in Paper II, where for model *S*, 19% of the collisions were the result of a dynamical encounter.

3.6 Supernovae

Supernovae can dramatically affect the evolution of a star cluster. During a supernova, the exploding star ejects a large fraction of its mass at high speed. This mass quickly leaves the cluster, as the ejection velocity far exceeds the cluster's escape speed. In addition, the newborn compact object may also receive a kick velocity large enough to escape the cluster. Binaries are very fragile to supernovae, and each binary hosting a supernova is likely to be dissociated.

3.6.1 Supernova types

Tables 5 and 6 present overviews of the supernovae observed in the models discussed in this paper, and compare them

Table 5. Observed supernova types (Obs, from Cappellaro et al. 1997) and supernovae occurring in a standard Scalo (1986) mass function (model IMF), the population synthesis calculations of model AK by Portegies Zwart & Verbunt (1996, model PZV-AK) and in models W4 and W6, and when the dynamical evolution of the stellar system is ignored (models W4-nd and W6-nd). The first column indicates the model, followed by the number of supernovae of types Ia, Ib, Ic and II. All numbers are normalized to 1.

model	Ia	Ib	Ic	II
Obs	0.09	0.11	0.18	0.62
IMF	—	—	0.12	0.88
PZV-AK	0.03	0.13	0.12	0.72
W4	0.22	0.20	0.07	0.50
W4-nd	0.06	0.20	0.17	0.57
W6	0.10	0.20	0.10	0.63
W6-nd	0.04	0.23	0.08	0.65

Table 6. Overview of the core-collapse supernovae which occurring in models W4 and W6. The progenitors are presented in the first column. When two stars are enclosed by parentheses, the left star explodes. Two stars enclosed by braces are the result of a merger or collision. The second column identifies the supernova type. Subsequent columns indicate how many core-collapse supernovae occurred in the models. The subdivisions *dyn* and *non-dyn* refer to models with and without dynamics. Superscript numbers indicate the numbers of binaries that survive the supernova. The rows below N_{esc} indicate the numbers of escapers experiencing a core collapse supernova *after* being ejected from the cluster. The table does not list the 3 stars in each model that collapse into black holes. The * indicates that one supernova occurred after a phase of mass transfer to a neutron star.

	Type	W4		W6	
	Type	dyn	non-dyn	dyn	non-dyn
Ntot:		38	35	25	26
wr	Ic	1	4 ²	0	2
gs	II	16	13	12	13
he	Ib	1	2	0	2 ¹
(gs, ms)	II	4	7	6	4
(gs, gs)	II	2	0	0	0
(gs, bh)	II	1	0	0	0
(he, ms)	Ic	3	2	2 ¹	0
(he, ms)	Ib	7 ¹	5	2	2 ¹
(he, he)	Ib	1	0	1	2
{wd, wd}	Ia	1	2	1	1
{gs, gs}	II	1	0	0	0
N_{esc}	total	16		6	
gs	II	2		1	
{wd, wd}	Ia	11		2	
(gs/he, ms)	Ib/II	2		3*	
{ms, ms}	II	1		0	

with expected supernova rates. Table 5 lists supernovae by type; Table 6 gives the evolutionary state of the exploding star and also indicates the possible presence of a binary companion. For comparison, we also present the expected number of supernovae given the same initial conditions, but ignoring the effects of dynamical evolution.

The adopted Scalo (1986) initial mass function contains

0.41 stars per thousand with $m > 25 M_{\odot}$ and 3.1 stars per thousand with $8 < m < 25 M_{\odot}$. In a naive evolution model, single stars with masses $\gtrsim 25 M_{\odot}$ may result in a Type Ic supernova, while stars more massive than $8 M_{\odot}$ produce a Type II supernova. For a population of 2000 single stars we then expect ~ 0.82 Type Ic and ~ 6.2 Type II supernovae. (Note that this estimate does not include binaries, and is therefore inapplicable to Type Ia and Ib supernovae.)

We compare these numbers with purely binary evolution models of Portegies Zwart & Verbunt (1996). According to their model AK, the Type Ic supernova rate is enhanced compared to models of only single stars. In the non-dynamical models (W4-nd and W6-nd), Type Ia and Ib supernovae occur without affecting the other supernova types. One reason for this is the fact that many Type Ib supernova originate from stars that were once part of a mass-transferring binary. The primary star in these binaries tends to lose its envelope in a phase of mass transfer and explode in a Type Ib supernova. The companion star, although initially not massive enough to experience a supernova, may accrete some material from the primary star. This accreted material may be sufficient to raise the secondary star's mass over the limit for experiencing a supernova. Stellar mass is, in a sense, recycled to produce more supernovae (see also Portegies Zwart & Yungelson 1999).

The relative numbers of supernova types Ia:Ib/c:II for the 8 model clusters (models W4 and W6 combined) are 0.18:0.27:0.55; in the models where stellar dynamics is ignored these ratio are 0.05:0.34:0.61. The addition of dynamical interactions to the models enhances the Type Ia supernova rate at the expense of the Type Ib/c and Type II supernova rates. The enhancement of Type-Ib/c supernova in model W4 is due to close (post mass transfer) binaries, possibly because these binaries experience more dynamical encounters during the shallow collapse of the cluster core (see the discussion in §3.1).

3.6.2 Binary survival rate

Only two binaries survive their first supernova. One remains bound because the supernova results in a black hole, which does not receive a velocity kick. This binary experiences a second phase of mass transfer (see §3.7 for details). The other surviving binary is the result of a supernova in a rather short-period binary with a main-sequence companion. The resultant neutron star receives only a mild kick and the binary remains bound. Later this binary becomes an X-ray source (see §3.7 for details).

Two supernovae are triggered by collisions between carbon stars, resulting in Type Ia events, and one Type II supernova follows a collision between two supergiants. One neutron star is shot into its $1.9 M_{\odot}$ main sequence companion following a supernova. The resulting collision product, a Thorn-Zytkow star, is ejected from the star cluster before collapsing to a black hole.

Only two out of 29 binaries survive the formation of a neutron star and one survives the formation of a black hole. A total of six black holes result from type Ic supernovae.

Figure 15 gives the time history of the supernovae in models W4 and W6. First black holes (bullets) are formed, followed by neutron stars (circles, triangles and plus signs). The supernovae in the W4 models seem to occur somewhat

earlier than in the W6 models, but the mean time at which a supernova occurs, 23.3 Myr and 23.5 Myr for models W4 and W6, respectively, are not significantly different. The formation of a black hole at 46 Myr in model W6 is the result of a radio pulsar colliding with its carbon-star companion (see §3.7).

3.7 Mass transfer and peculiar binaries

3.7.1 First Roche-lobe contact

The high binary fractions in our models result in frequent episodes of mass transfer. This is illustrated in Figure 16, which shows the distribution of the times of first Roche-lobe contact in models W4 and W6. The various symbols indicate the state of the donor at the moment of first contact. (Note that helium stars, although likely to be the remnant of an earlier phase of mass transfer, are still counted in this figure.)

In most cases the mass is transferred to a main-sequence star, except in the cases indicated with \times , where the mass transfer is onto a compact object (mostly a white dwarf). In the majority of these latter cases the donor is a (sub)giant, but there are two occasions where the donor is a helium star, and in one case a main-sequence star (see Figure 17. One episode of mass transfer occurs between a (sub) giant and a black hole (model W4 at $t = 829$ Myr).

The time histories of models W4 are significantly different from those of models W6, according to a χ^2 test on the cumulative distributions of Figure 16. In the W4 models, mass transfer tends to occur earlier than in the W6 models. As discussed above, the difference is a result of the greater dynamical activity during the early phase of model W4. In fact, the higher binary activity in this case is caused by the early phase of shallow core collapse in the W4 models, which does not occur in the W6 models.

3.7.2 X-ray binaries

Mass transfer from a hydrogen- or helium-burning star onto a compact object generally leads to an X-ray phase. Figure 17 shows the distribution of orbital periods (in days) at the onset of Roche-lobe overflow for binaries with white-dwarf (in one case a black hole) accretor. Note the clear distinction between main-sequence and helium-star donors at short orbital periods and giant donors at larger periods. The wide systems with giant donors are probably most comparable to the supersoft sources (X-ray binaries where a white dwarf accretes at a super-Eddington rate for a solar-mass object, emitting at a rate of about 10^{38} erg/s).

A peculiar object which might be observable as an X-ray source results from a binary in which a helium giant ($2.5 M_{\odot}$) transfers mass to a $1.17 M_{\odot}$ carbon-oxygen white dwarf. First contact occurs at 45.9 Myr at an orbital period of 1.7 days. When the carbon star explodes and becomes a neutron star (at 46.07 Myr) it receives a kick of only 16 km s^{-1} . At that moment the companion star still fills its Roche lobe, and as a result the two stars coalesce into a single object. The merger product collapses a little later to form a $2.42 M_{\odot}$ black hole.

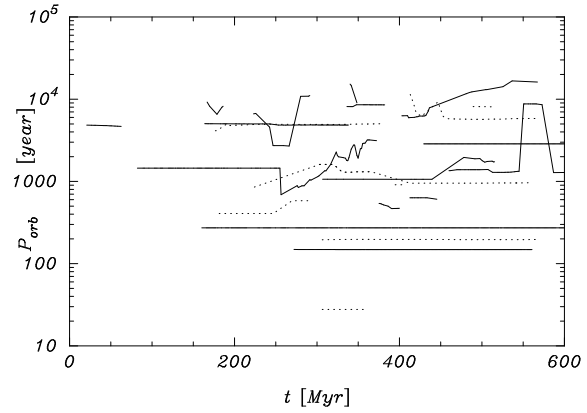


Figure 18. Orbital periods of the outer components of all hierarchical triples in all models, solid curves for the multiples in models W4, the dotted lines for the W6 multiples.

3.8 Triples and higher order systems

Long-lived triples and higher-order systems pose severe challenges to any numerical code. We encountered a total of 41 long-lived multiples in our runs, 21 triples [4 quadruples] in W4 and 13 triples [3 quadruples] in W6. Only one of the quadruple systems is hierarchical; the others are binary-binary systems.

The first multiple systems form as early as 20 Myr (by a binary-binary interaction); some survive for as long as 900 Myr. Figure 18 presents an overview of all triples in all models from $t = 0$ to 600 Myr. (At later times the numbers of triples decrease as the clusters dissolve.) The orbital period of the outer binary is generally rather constant. This is not surprising as, for the triple to be long-lived, it must be hierarchical and isolated, and the orbital energies and hence periods are adiabatic invariants. The systems showing a significant period derivative are driven by binary evolution or by temporary close encounters with other cluster members.

The fractions of long-lived triple and quadruple systems in our models are only $\sim 0.26\%$ and $\sim 0.12\%$, respectively, considerably smaller than the fraction of triples observed in the Galactic field (2.6%, Duquennoy & Mayor 1991) or in the Pleiades cluster ($\sim 2\%$, Mermilliod et al. 1990, 1992). Note also that these are the total numbers of multiple systems created at any time during our simulations. The mean lifetime of such a system is 280 ± 180 Myr.

We can study the population of short-lived multiple systems by selecting a bound pair of stars and searching for a third nearby star which forms a bound subsystem. At any moment in time the number of such short-lived multiple systems is about twice as high as the number of persistent triples. At $t = 600$ Myr we counted a total of 46 bound multiple systems in all models (W4 and W6), implying in a triple frequency of about 0.6% per star. For comparison, Kroupa (1995) found a triple fraction of 0.5% using a similar technique. The outer orbits of these triples, however, are generally rather soft.

Nine collision products in our models W4 became members of persistent triples or quadruples. These collisions occurred in transient triples. In about half (5) the cases, the two stars in the inner binary collided while the intruding star remained bound to the merged star. (For definiteness,

Model

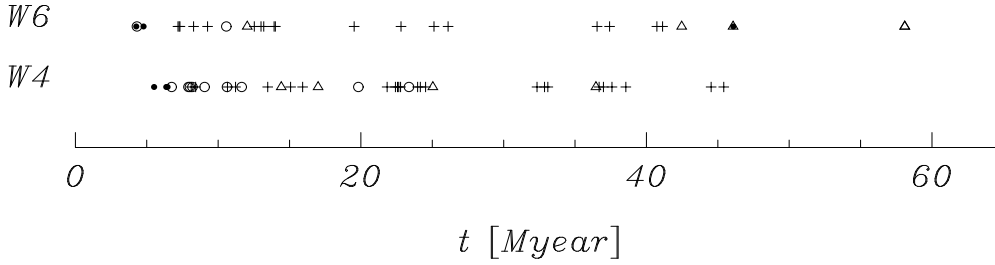


Figure 15. Supernova history for models W4 (bottom) and W6 (top). Type Ib, Ic and II supernovae are identified with circles, triangles, and plus-signs, respectively. Black-hole formation is identified with \bullet . Note the collapse of a neutron star to a black hole in one of the W6 models around $t \sim 46$ Myr (filled triangle). The time histories of these two distributions are not significantly different.

Model

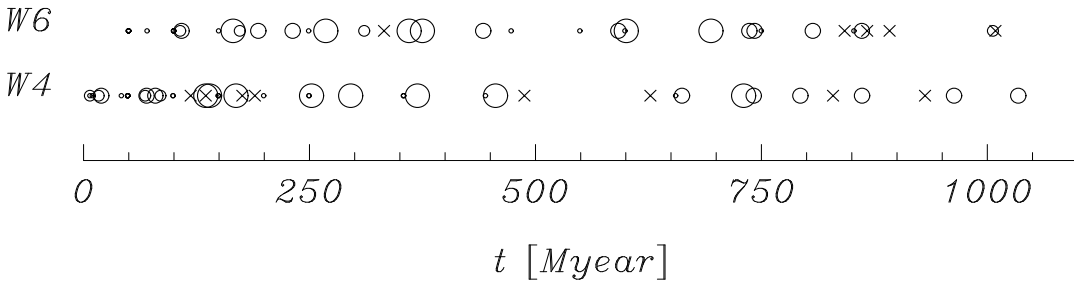


Figure 16. Times of first mass transfer for binaries in models W4 and W6. The circle size indicates the evolutionary state of the donor, from main-sequence (small) via Hertzsprung gap, and sub-giant, with supergiant indicated by the largest circles. The \times symbols indicate mass transfer onto a white dwarf (or a black hole, for the second \times from the right in model W4).

we take the “inner” orbit in a quadruple system to be the larger of the two inner orbits.) In a few cases (3), the merger product and its companion became bound to another third star, forming a stable triple. In two of these cases, the encounter resulted in second collision with the merger product. Both these triple collisions resulted in blue stragglers which had, at some time, a mass exceeding twice the turnoff mass of the cluster.

Of the total of 117 collisions in the W4 models, nine occurred in transient triple systems. With a triple frequency of only $\sim 0.26\%$, one naively expects less than one collision to occur in triples, making the frequency of collisions in triples unusually high. In part, this higher fraction of collisions in multiples is due to the dynamics—such systems generally form close to the cluster center, where the stellar density is highest and most collisions are expected. In addition, collision products tend to be found near the center, because they are more massive than average. The higher combined mass of three stars and the relatively large cross section of the outer orbit also increases the collision probability. Similar circumstances led to the high collision rates observed in the R 136 simulations of Portegies Zwart et al. (1999, see also Portegies Zwart & McMillan 2002). Thus, triples are favorable for collisions, and collision products favor triple systems.

We can characterize the triple systems formed in our simulations as follows: All inner orbits have periods less than

100 year with an average of about 5.1 years. All outer orbital periods exceed 100 year and have an average of about 4600 years. The eccentricities of the inner and outer orbits are quite distinct. The inner orbits have generally rather small eccentricities ($e = 0.44 \pm 0.3$) and its distribution is consistent at a 98.8% level with the inner eccentricity distribution of observed triples (Tokovinin 1997). The distribution of outer eccentricities ($e = 0.65 \pm 0.14$) is consistent with thermal.

4 COMPARISON WITH PREVIOUS WORK

4.1 McMillan & Hut 1994

The simulations reported by McMillan and Hut (1994) used up to 2048 stars, with up to 20% (rather soft: $1 - 20$ or $1 - 100kT$) primordial binaries, and included the Galactic tidal field. However, they excluded stellar evolution and hence any stellar mass loss. In the absence of a physical time scale associated with stellar evolution, they presented their results in units of the initial relaxation time. Our W6 models have half lives of about 6 initial relaxation times, much shorter than the $\sim 12-30$ initial relaxation times for the most comparable McMillan & Hut models. Stellar mass loss is the main reason for the more rapid dissolution of our models; in addition, the McMillan & Hut runs all began with the cluster well inside its Jacobi surface, so the clusters had to expand significantly before significant tidal mass loss

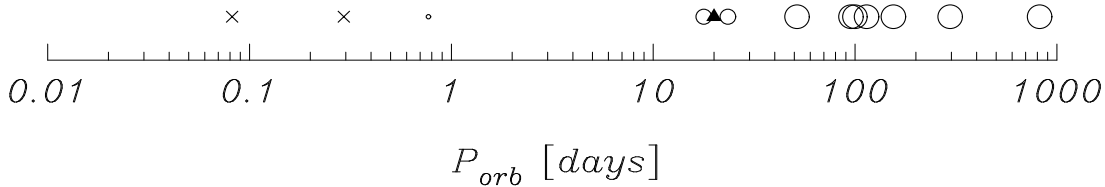


Figure 17. Orbital period (in days) at the onset of mass transfer onto a compact object, for models W4 and W6. The circle size indicate the evolutionary state of the donor, from main sequence (smallest circles) to supergiant (large circles). The \times indicates that the donor is a helium star; the filled triangle indicates the period of the single black hole X-ray binary.

occurred. As discussed previously, all the McMillan & Hut models experienced core collapse, which is not seen in our simulations, where core collapse is arrested by stellar mass loss.

McMillan & Hut found that the binary fraction in their simulations first fell due to as binaries were destroyed by interactions with other binaries in the cluster core, then rose again at late times as the cluster evaporated in the Galactic tidal field. In contrast, we find that the (initially $\sim 50\%$) binary fraction in our models remains roughly constant throughout the calculation, then increases significantly to $\sim 70\%$ when only $\sim 10\%$ of the cluster mass remains. These differences are most likely attributable to the lack of significant core collapse and the stronger tidal fields in our runs.

One of the most interesting conclusions made by McMillan & Hut is that the spatial distribution of hard binaries is different than the distribution of soft binaries (see their Figure 9). In Figure 7 we showed that hard binaries $E > 1000kT$ are slightly more centrally concentrated than average.

4.2 Kroupa 1995

The main difference between our calculations and those of Kroupa (1995) is his neglect of binary evolution and his inclusion of a prescription for pre-main-sequence binaries. The eccentricity distribution of his 'primordial' binaries was therefore somewhat different from ours, but this affects only binaries with the highest eccentricities and the shortest orbital periods. On the other hand, his neglect of binary evolution underestimated the fraction of tidally circularized binaries. In his calculations the boundary between hard and soft binaries was at an orbital period of roughly 2.7×10^4 years, similar to that in our models W4. We have already compared the characteristics of the populations of triple systems in our calculations (see §3.8).

4.3 De La Fuente Marcos 1997

De la Fuente Marcos (1997) performed studies of the evolution of small ($N \leq 750$), tidally limited open clusters having a variety of initial mass functions, with and without the inclusion of stellar (but not binary) evolution. All models started with a substantial fraction ($1/3$) of primordial binaries having mass ratios of 0.5 and energies in the $\sim 1-10kT$ range. He found that the dissolution time scale of his models depended quite sensitively on the choice of IMF, and that the binary population shortly before dissolution could

show characteristic features allowing remnants of rich and poor clusters to be distinguished observationally. It is unclear how these results extend to larger systems.

The binary fraction in the de la Fuente Marcos simulations ranged from 33% initially to about $51\% \pm 0.19\%$ near the disruption of the cluster (averaged over all 20 of his simulations). By the time the clusters dissolved, the binary fraction in the core had dropped to $15\% \pm 0.13\%$. We find a similar increase in the total binary fraction, but clearly the core binary fraction in our models is much higher (see Figure 7). The small binary fractions in the core near the end of his simulations are the direct result of his choice of initial binary binding energies.

4.4 Papers I, II

The comparison between the relative collision frequencies in Tab. 4 and those of model *S* in Paper I are quite striking. In that paper only encounters between single stars were studied and primordial binaries were neglected. Still, in Paper I 77% of all collisions occurred between two main-sequence stars, and 14% between a main-sequence star and a giant; the remaining 9% involved giants and remnants.

The (ms, ms) merger rates in our models are comparable to the merger rates in paper II, but (ms, wd) were much greater in model *S* of paper II because it is older (10Gyr). The (ms, gs) merger rate is lower because there are fractionally fewer main-sequence stars in paper II.

4.5 Hurley et al. 2001

Hurley et al. (2001) have modeled the open cluster M67, using a simulation code similar in many ways to our own. Both codes use fitting formulae for single star evolution, and include a series of recipes for dealing with binary star evolution. The main difference between Hurley et al. (2001) and the current paper lies in the parameter choices for their simulations: they evolved 15,000 stars to an age of 2500 Myr, before adding dynamics, in the form of a direct N -body calculation. They then evolved the combined model to an age of 4300 Myr, appropriate for the old open cluster M67. They also present the results from smaller N -body runs, starting at earlier times.

Hurley et al. (2001) focused mostly on the formation of blue stragglers, and reported that their simulations indeed produced roughly the right number of blue stragglers, in agreement with observations of M67. They also performed a non-dynamical binary evolution population synthesis, and found that the number of blue stragglers in that case fell

short of that required by observations. They concluded that dynamical encounters have been crucial in the evolution of M67. While it is difficult to make a quantitative comparison between their simulations and ours, given the rather different types of initial conditions, our main results concerning the numbers and types of collisions, and the formation rate of triples are in broad agreement.

5 SUMMARY AND CONCLUSIONS

We have performed detailed N -body calculations of intermediate-mass open clusters near the Sun. The initial conditions were selected to mimic star clusters such as Pleiades, Praesepe and Hyades. Our calculations included the effects of dynamical encounters between stars and higher order systems, the tidal field of the parent Galaxy and the evolution of single stars and binary stars.

5.1 Cluster lifetime and structure

Our model star clusters dissolved in the tidal field of the Galaxy within about 1 billion years. The rate of mass loss remained roughly constant, at ~ 0.8 – $1.4 M_{\odot}$ per million years, corresponding to a cluster half-life of ~ 600 – 1000 Myr, depending on distance from the Galactic center.

The density profiles of the model clusters changed dramatically during the cluster lifetime. Core collapse was prevented by stellar mass loss and binary heating. Our less concentrated (W4) models became more compact during the first few million years, whereas the more concentrated (W6) models expanded from the beginning. The W4 models still dissolved more quickly in the Galactic tidal field, however, mainly due to their closer proximity of the Galactic center.

Mass segregation is a very efficient process. After only a small fraction of an initial relaxation time, single white dwarfs, giants, collision products, hard binaries, mass transferring binaries and binaries with one or two massive components (compared to the mean mass in the cluster) were all noticeably more centrally concentrated than the average star, as measured by the half mass radii of the various components.

5.2 Binary stars

The numbers of binaries decreased with time at roughly the same rate as the numbers of single stars, with the result that the binary fractions in our models remained more or less constant over the studied range of cluster ages. The binary fraction generally decreased during the first few million years by several percent, due to supernovae and dynamical encounters, both of which tended to disrupt binaries. For the remainder of the evolution, this fraction slowly increased. The maximum binary fraction of $\sim 65\%$ is reached near disruption. The fraction of binaries in the core remained between 50% and 60% higher than the fraction near the half-mass radius over the entire lifetime of the cluster.

The widest binaries were dissociated soon after the start of the simulations. A considerable fraction ($4.5 \pm 0.6\%$) of highly eccentric binaries with rather short orbital periods circularized and some experienced mass transfer early in the evolution of the cluster. These short-period binaries were

generally more centrally concentrated than wider binaries or single stars, because they are on average more massive than single stars and do not interact.

The overall distributions of binary parameters, however, hardly change with time. Apart from the loss of binaries with the largest orbital periods and those with short orbital periods and high eccentricities, most binaries were relatively unaffected by either stellar evolution or stellar dynamics. The observed binary populations in open clusters may therefore be a reasonable representation of the initial primordial population.

5.3 Escapers

We define three families of escaping stars. (1) Neutron stars were ejected from the cluster with very high velocities. About 0.4% of all stars were ejected as neutron stars due to supernova explosions. (2) Massive stars tended to have rather high escape velocities, because they were often found in close binaries which were disrupted by the explosion of the primary star, possibly after a phase of mass transfer. The average escape velocity of all single main sequence stars in model W4 was $v_{\text{esc}} = 1.2 \pm 0.51 \text{ km s}^{-1}$, whereas stars with $m \gtrsim 4 M_{\odot}$ had $v_{\text{esc}} = 17.4 \pm 2.3 \text{ km s}^{-1}$. For model W6 these numbers are only slightly smaller. (3) The mean escaper velocity of low-mass stars ($v_{\text{esc}} = 1.0 \pm 0.28 \text{ km s}^{-1}$ for stars with $m < 0.5 M_{\odot}$) was comparable to the cluster velocity distribution; the mean velocity of escaping binaries was ($v_{\text{esc}} = 0.97 \pm 0.29 \text{ km s}^{-1}$ for model W4 and $v_{\text{esc}} = 0.81 \pm 0.29 \text{ km s}^{-1}$ for model W6), somewhat smaller than that for single stars.

5.4 Stellar collisions

Not surprisingly, collisions tended to occur near the cluster center, but a considerable fraction of mergers occurred farther out, near the tidal radius. More than 80% of all collisions occurred within about two core radii. Most ($\sim 80\%$) collisions occurred between two main sequence stars. About 70% of the collisions were the result of an unstable phase of mass transfer. The rest occurred in single-star–binary or binary–binary encounters. Multiple collisions were rare: only two out of 241 in our model calculations.

Collision participants were somewhat more massive than expected based on the simple cross section arguments presented in Paper III. Most (85%) collisions occurred between main-sequence stars; most of the remainder involved a main-sequence star and a giant (12%). Only 3% of the collisions occurred between two remnants. The dynamical activity in the cluster core, however, caused quite a few white dwarfs to become binary members, which would later merge due to the emission of gravitational waves. This leads to a rather high merger rate among white dwarfs (see also Shara & Hurley 2002).

5.5 Supernovae and stellar remnants

The overall supernova rate in our simulations was consistent with rates observed in the Galaxy. However, the ratios of Type II to Type Ia, Ib, and Ic supernova are quite different. Most striking is the order of magnitude enhancement

of type Ia supernovae in the W4 models compared to the non-dynamical models and the population synthesis of non-interacting binaries. In these same models, Type Ib supernova are enhanced by about a factor of two compared to a population of binaries without dynamical encounters.

Because of the assumed neutron-star kick distribution, pulsars were generally not retained in our cluster models. Only one out of 61 neutron stars was retained to form an X-ray binary later in its lifetime. The observed velocity distribution of ejected pulsars was somewhat smaller than the input kick velocity distribution. X-ray binaries in which a white dwarf accretes from a companion star were about an order of magnitude more common. X-ray binaries containing black holes were rare simply because such objects form from the highest-mass stars, which are themselves rare.

Among the more unusual collisions, in our simulations, we observed one between a neutron star and a helium giant, two between CO white dwarfs, resulting in type Ia supernovae and the formation of an X-ray binary with a black hole as accretor. Several white dwarfs experienced a phase of mass transfer from a companion star. The donor was most often a (sub)giant. In total, 13 X-ray binaries were formed, most with a white dwarf as accretor.

5.6 Multiple systems

The number of persistent triples formed in our calculations was about an order of magnitude smaller than the observed fraction of triples in open clusters and the Galactic disk, although the frequency of triples and higher-order systems present at any moment in our simulations was comparable to the numbers actually observed. The majority of these were transient, however, and their orbital parameters differed considerably from observations. The orbital parameters of the outer orbits of the formed triples formed in our models was not representative of triples observed in the Galaxy, which tend to have shorter periods and lower eccentricities.

ACKNOWLEDGMENTS

This work was supported by NASA through Hubble Fellowship grant HF-01112.01-98A (NASA contract NAS 5-26555) by the Space Telescope Science Institute, the Royal Netherlands Academy of Sciences (KNAW), the Netherlands organization for scientific research (NWO), by NASA ATP grants NAG5-6964 and NAG5-9264. Calculations were performed on the GRAPE-4 systems at Tokyo University, Drexel University and the University of Bloomington. SPZ is grateful to Drexel University, Tokyo University and the Institute for Advanced study for their hospitality.

REFERENCES

- Abt, H. A., Levy, S. G. 1972, *ApJ*, 172, 355
 Andrievsky, S. . M. 1998, *A&A*, 334, 139
 Blaauw, A. 1961, *ban*, 15, 265
 Bouvier, J., Rigaut, F., Nadeau, D. 1997, *A&A*, 323, 139
 Cox, A. N. 1954, *ApJ*, 119, 188
 Dachs, J., Kabus, H. 1989, *A&As*, 78, 25
 Drukier, G. A., Slavin, S. D., Cohn, H. N., Lugger, P. M., Berrington, R. C., Murphy, B. W., Seitzer, P. O. 1998, *AJ*, 115, 708
 Duquennoy, A., Mayor, M. 1991, *A&A*, 248, 485
 Frandsen, S., Dreyer, P., Kjeldsen, H. 1989, *A&A*, 215, 287
 Gies, D. R., Bolton, C. T. 1982, *ApJ*, 260, 240
 Harris, G. L. H., Fitzgerald, M. P. V., Mehta, S., Reed, B. C. 1993, *AJ*, 106, 1533
 Hartman, J. W. 1997, *A&A*, 322, 127
 Hartwick, F. D. A., Hesser, J. E. 1971, *PASP*, 83, 53
 Hawley, S. L., Tourtellot, J. G., Reid, I. N. 1999, *AJ*, 117, 1341
 Heggie, D. C., Ramamani, N. 1995, *MNRAS*, 272, 317
 Hodgkin, S. T., Pinfield, D. J., Jameson, R. F., Steele, I. A., Cossburn, M. R., Hambly, N. C. 1999, *MNRAS*, 310, 87
 Hurley, J. R., Tout, C. A., Aarseth, S. J., Pols, O. R. 2001, *MNRAS*, 323, 630
 Hurley, J. R., Tout, C. A., Pols, O. R. 2002, *MNRAS*, 329, 897
 Ianna, P. A., Adler, D. S., Faudree, E. F. 1987, *AJ*, 93, 347
 Jones, B. F., Stauffer, J. R. 1991, *AJ*, 102, 1080
 Kroupa, P. 1995, *MNRAS*, 277, 1522
 Makino, J. 1991, *ApJ*, 369, 200
 Makino, J., Aarseth, S. J. 1992, *PASJ*, 44, 141
 Makino, J., Taiji, M., Ebisuzaki, T., Sugimoto, D. 1997, *ApJ*, 480, 432
 McMillan, S., Hut, P., Makino, J. 1990, *ApJ*, 362, 522
 McMillan, S., Hut, P., Makino, J. 1991, *ApJ*, 372, 111
 McMillan, S. L. W. 1986a, *ApJ*, 306, 552
 McMillan, S. L. W. 1986b, *ApJ*, 307, 126
 McMillan, S. L. W., Hut, P. 1996, *ApJ*, 467, 348
 Mermilliod, J. C., Mayor, M. 1999, in 10 pages, 3 tables, 7 eps figures. Accepted for *A&A*; *LaTeX Preprint no. IAUL preprint no 85.*, 11405
 Mermilliod, J. C., Rosvick, J. M., Duquennoy, A., Mayor, M. 1992, *A&A*, 265, 513
 Mermilliod, J. C., Weis, E. W., Duquennoy, A., Mayor, M. 1990, *A&A*, 235, 114
 Nordstroem, B., Andersen, J., Andersen, M. I. 1996, *A&As*, 118, 407
 Nordstroem, B., Andersen, J., Andersen, M. I. 1997, *A&A*, 322, 460
 Perryman, M. A. C., Brown, A. G. A., Lebreton, Y., Gomez, A., Turon, C., De Strobel, G. C., Mermilliod, J. C., Robichon, N., Kovalevsky, J., Crifo, F. 1998, *A&A*, 331, 81
 Pinfield, D. J., Jameson, R. F., Hodgkin, S. T. 1998, *MNRAS*, 299, 955
 Portegies Zwart, S. F. 2000, in *ApJ* in press., 5202
 Portegies Zwart, S. F., Hut, P., Makino, J., McMillan, S. L. W. 1998, *A&A*, 337, 363
 Portegies Zwart, S. F., Hut, P., Verbunt, F. 1997, *A&A*, 328, 130
 Portegies Zwart, S. F., Makino, J., McMillan, S. L. W., Hut, P. 1999, *A&A*, 348, 117
 Portegies Zwart, S. F., Makino, J., McMillan, S. L. W., Hut, P. 2001, *ApJ*, 546, L101
 Portegies Zwart, S. F., McMillan, S. L. W. 2002, *ApJ*, 576, 899
 Portegies Zwart, S. F., van Den Heuvel, E. P. J. 1999, *New Astronomy*, 4, 355
 Portegies Zwart, S. F., Verbunt, F. 1996, *A&A*, 309, 179

- Portegies Zwart, S. F., Yungelson, L. R. 1998, *A&A*, 332, 173
Portegies Zwart, S. F., Yungelson, L. R. 1999, *MNRAS*, 309, 26
Raboud, D., Mermilliod, J. C. 1998, *A&A*, 329, 101
Reid, I. N., Hawley, S. L. 1999, *AJ*, 117, 343
Sandrelli, S., Bragaglia, A., Tosi, M., Marconi, G. 1999, *MNRAS*, 309, 739
Scalo, J. M. 1986, *Fund. of Cosm. Phys.*, 11, 1
Shara, M. M., Hurley, J. R. 2002, *ApJ*, 571, 830
Stone, R. C. 1991, *AJ*, 102, 333
Tokovinin, A. A. 1997, *A&As*, 124, 75
van Den Hoek, L. B., de Jong, T. 1997, *A&A*, 318, 231

This paper has been typeset from a \TeX / \LaTeX file prepared by the author.